Indirect urea electrooxidation by nickel(III) in alkaline medium: From kinetic and mechanism to reactor modeling

Guillaume Hopsort, Laure Latapie, Karine Groenen Serrano, Karine Loubière, Theodore Tzedakis

Received: 21 December 2022 | Revised: 9 March 2023 | Accepted: 2 April 2023

DOI: 10.1002/aic.18113

AIChE JOURNAL

RESEARCH ARTICLE

Reaction Engineering, Kinetics and Catalysis

Indirect urea electrooxidation by nickel(III) in alkaline medium: From kinetic and mechanism to reactor modeling

Guillaume Hopsort | Laure Latapie | Karine Groenen Serrano | Karine Loubière | Theodore Tzedakis

Laboratoire de Génie Chimique, Université de Toulouse, CNRS, INPT, UPS, Toulouse, France

Correspondence
Theodore Tzedakis and Guillaume Hopsort, Laboratoire de Génie Chimique, Université de Toulouse, CNRS, INPT, UPS, Toulouse, France.
Email: theodore.tzedakis@univ-tlse3.fr and guillaume.hopsort@univ-tlse3.fr

Funding information
Agence Nationale de la Recherche, Grant/Award Number: HYUREA ANR-19-CE04-0009

Abstract

This study consists in the determination of two kinetic laws of urea oxidation (UO) and electrooxidation (UEO) in alkaline media on nickel(III). Two kinds of active sites were examined, the first one derived from a $Ni(OH)_2$ powder and the second from a massive nickel electrode. Partial orders of nickel(III) (two for UO and five UEO) enable to conclude about (i) the urea adsorption on two nickel(III) sites and (ii) that a multistep oxidation of urea occurs involving five nickel(III) site electroregenerations. A multipathway mechanism is also proposed to explain UEO facilitated by the nickel(III)/nickel(II) mediation system, and to predict the by-products' formation previously identified (NO_2^-, NH_3, OCN^-, CO_3^{2-}). At last, a model combining the UEO kinetic law previously established, with diffusive and convective transport phenomena was developed. A consistent correlation (maximum deviation of 6%) between laboratory electrolysis results with the model' predictions was obtained under different operating conditions, enabling the validation of this model.

KEYWORDS
heterogeneous coupled reactions, mechanism and kinetics, Ni(III)/Ni(II) mediator, transport phenomena modeling, urea electrooxidation

1 | INTRODUCTION

Wastewater treatment and energy issues are nowadays major societal problems requiring numerous investments. Previously considered as waste, fresh water, that is, contaminated by human activity (carbon industry, transportation, etc.) and by the primary sector (mining and agriculture) is now recognized as a significant source of pollutants valorization. Interest is enhanced as the waste water production is expected to increase by about 50% by the year 2050.[1] Containing urea (40% wt.,[2] at around 0.33 mol L^{-1}), urine constitutes an important source of nitrogen, accounting for nearly 75% of the nitrogen in watercourses.[3] Electrochemical oxidation of urea is nowadays studied for meeting various targets, such as electrolyzers[4–7] (producing H_2 as an energy carrier), energy production by urea fuel cells,[8–13] or the development of advanced electrode materials.[14–17] Recent investigations[18,19] have claimed that low-cost electrode materials could be used in alkaline media for efficient urea electrooxidation (UEO), thus opening promising perspectives for UEO implementation on an industrial scale. In particular, nickel oxides exhibit important catalytic activity regarding urea oxidation in presence of hydroxide ions, which enables a simplified reaction scheme[20–22] described by Equations (1)–(5) to be proposed.

(i) At the anode:

$$\left\{Ni(OH)_{2,(s)} + OH^-_{(aq)} \leftrightarrow NiOOH_{(s)} + e^- + H_2O_{(l)}\right\} \times 6 \quad (1)$$

$$CO(NH_2)_{2,(aq)} + H_2O_{(l)} + 6NiOOH_{(s)} \rightarrow 6Ni(OH)_{2,(s)} + N_{2,(g)} + CO_{2,(g)} \quad (2)$$

(ii) Anodic overall:

$$CO(NH_2)_{2,(aq)} + 6OH^-_{(l)} \rightarrow N_{2,(g)} + 5H_2O_{(l)} + CO_{2,(g)} + 6e^- \quad (3)$$

(iii) At the cathode:

$$6H_2O_{(l)} + 6e^- \rightarrow 3H_{2,(g)} + 6OH^-_{(aq)} \quad (4)$$

(iv) Overall:

$$CO(NH_2)_{2,(aq)} + H_2O_{(l)} \rightarrow N_{2,(g)} + 3H_{2,(g)} + CO_{2,(g)} \quad (5)$$

The redox system $NiOOH/Ni(OH)_2$ acts as a redox mediator catalyzing urea mineralization.[23] In such a system, nickel peroxide, NiOOH, is constantly regenerated at the electrode surface by an electrochemical reaction (ER, Equation (1)). Six electrons, supplied by 6 NiOOH, are required to achieve a complete mineralization (i.e., to be converted into CO_2 and N_2) of one urea molecule according to a heterocatalytic chemical reaction (HCR, Equation (2)). However, recent works have provided new insights on urea oxidation by demonstrating that, beyond the formation of N_2, various by-products are produced, such as cyanate, nitrite, ammonium, and carbonate ions.[24,25]

A deeper knowledge of the reaction scheme coupled to the determination of kinetic laws and the related parameters remain a prerequisite to design and to operate UEO processes on an industrial scale.[26,27] To the best of our knowledge, only two studies have been devoted to these investigations. By neglecting the catalytic regeneration of the couple $NiOOH/Ni(OH)_2$ and using Tafel plots, Vedharathinam et al.[28] were the first to propose the following simplified kinetic law as in Equation (6) without determining the kinetic constant k.

$$Rate_{urea} = k \times \left[CO(NH_2)_2\right]^{0.3} \times [OH^-]^2 \quad (6)$$

Later, partial orders of 1.22 and 0.26 for hydroxide ions and urea respectively on a β-NiOOH covered electrode were obtained using cyclic voltammetry and Tafel plots by Singh et al.[29] The authors have claimed that: (i) the reaction order of urea concentration is independent of the applied potential and (ii) increasing the applied potential causes the reaction order of the hydroxide ions to decrease. However, in these studies, experiments were carried out in transient state conditions (i.e., high potential scan rate ν_{scan}), in which nickel(III) was not constantly regenerated at the electrode surface, as pointed out in our previous study.[30] As obtained in the mixed ER/HCR regime and at low urea conversion rates, the related values of partial reaction orders allowed neither the understanding of the impact that the secondary reactions (occurring at higher urea conversion rates) may have on the electrochemical system, nor obtaining access to relevant intrinsic kinetic information.

To fill this gap, this paper aims at investigating the kinetics of NiOOH catalytic urea oxidation in an alkaline medium. For this purpose, and since neither explicit rate law nor kinetic models are described in the literature, a novel approach will be suggested, combining studies of the urea action according to (i) specifically synthesized NiOOH powder and to (ii) electrochemically generated NiOOH sites, carried out under steady state conditions. By implementing catalytic urea oxidation in a suspension of NiOOH solid particles, one can expect to bring new insights on the reaction kinetics by comparing physico-chemical phenomena taking place in the presence of (i) nonregenerated NiOOH sites (adsorption, HCR, desorption) on solid particles or (ii) electrogenerated NiOOH sites (HCR/ER coupling). Results on oxidation kinetics with the synthesized nickel particles will first be studied. The experiments performed in a lab-scale electrolysis cell at low scan rates enabled to determine the key parameters of the kinetic law for the UEO reaction. Furthermore, by combining the newly established kinetic rate law with the electrolysis results obtained at high urea conversion rates, a detailed mechanism of urea oxidation in alkaline medium on nickel(III) active sites was proposed, allowing the formation of the liquid phase by-products identified by Tatarchuk et al.[25] and also in our previous work.[30] Finally, one can regret a lack of Electrochemical Engineering approach of the UEO processes (cell design, geometry and optimization at pilot and industrial scale)[31,32] in the state of the art. The present study proposes an original approach enabling the coupled phenomena (electrooxidation, adsorption, kinetic and mass transport) that occurs during the UEO process to be described. This approach is based on: (i) the rigorous determination of the kinetic law; (ii) the establishment of the multipathway mechanism responsible for the formation of all the liquid phase by-products; and (iii) a robust (maximum deviation of 6%) predictive model which, to the knowledge of the authors, has never been applied to UEO. This model will predict the conversion rate of urea during electrolysis at high conversion rates and on a large scale.

Section 2 describe (i) the synthesis pathway of the NiOOH powder and the associated characterization techniques, (ii) the set-up and the analytical technique to monitor the reaction between urea and nickel(III) particles and, (iii) the electrochemical set-up. Section 3 discusses the kinetic parameters deduced from both chemically and electrochemically synthesized nickel(III) particles, and then elucidates the UEO mechanism. Finally, Section 4 is dedicated to the construction of a model, that is, able to predict the temporal variation of urea conversion during batch electrolysis and its validation by comparison with experimental data.

2 | EXPERIMENTAL

Details concerning chemicals (Normapur® grade) are reported in Section S1 (refer to Table S1).

2.1 | NiOOH catalyst powder

2.1.1 | Synthesis

The NiOOH powder was synthesized following the protocols developed by Pan et al.[33] and Thimmasandra et al.[34] They consisted of oxidizing a $Ni(OH)_2$ powder at room temperature in the presence of sodium hypochlorite NaOCl and sodium hydroxide NaOH, as Equation (7):

$$Ni(OH)_{2,(s)} + OCl^-_{(aq)} \rightarrow NiOOH_{(s)} + \frac{1}{2}Cl_{2,(g)} + OH^-_{(aq)} \quad (7)$$

Specifically, NiOOH particles were prepared by mixing 5 g of a commercially available nickel powder (refer to Section S1) with a solution containing 400 mL of sodium hypochlorite and 2 g of sodium hydroxide. The reaction was achieved after 4 h of magnetic stirring, then the mixture obtained was filtered using a Büchner sintered glass filter; the substance was then washed with 6 × 60 mL of deionized water. The NiOOH powder was finally dried in an oven at a temperature of 80°C for 3 days.

Two different concentrations of hypochlorite (1.76×10^{-1} mol L^{-1} and 7.68×10^{-1} mol L^{-1}) powders, sample 1 and sample 2 respectively, were synthesized to vary the nickel(III) purity.

2.1.2 | Characterization

Various techniques were used to characterize the initial and the synthesized powders. For sake of clarity, all the results obtained from these methods are reported in Section S2.

First, the purity of the nickel(III) particles was quantified by potentiometric back titration using Mohr's salt. An excess of ferrous salt was introduced into a suspension of $NiOOH/Ni(OH)_2$ particles. After reaction, the excess of ferrous salt was titrated by an acidic solution of potassium dichromate in accordance with Equations (8) and (9).

$$NiOOH_{(s)} + Fe^{+II}_{(aq)} + 3H_3O^+_{(aq)} \leftrightarrow Ni^{2+}_{(aq)} + Fe^{+III}_{(aq)} + 5H_2O_{(l)} \quad (8)$$

$$6Fe^{+II}_{(aq)} + Cr_2O^{2-}_{7,(aq)} + 14H_3O^+_{(aq)} \leftrightarrow 2Cr^{3+}_{(aq)} + 6Fe^{+III}_{(aq)} + 21H_2O_{(l)} \quad (9)$$

The purity was determined as the ratio of the mass of nickel(III) deduced from the titration to the initial mass of the $Ni(OH)_2$ powder used in the trial. The set-up related to these experiments is schematically described in Figure S2.

The crystalline structure of the nickel synthesized powders was studied by XRD analysis using a diffractometer (MiniFlex600-D/Tex Ultra2, Rigaku®, Japan) with Cu Kα radiation (40 kV, 15 mA). Data, illustrated in Figure S4, were collected in the 2θ range of 5°–92°. The step width was 0.02° with a scan speed of 10°min^{-1}. From the literature on nickel(III) XRD characterizations,[34–38] the initial powder was well identified as nickel(II) hydroxide β-$Ni(OH)_2$ with a brucite-type structure. After synthesis, samples 1 and 2 were found to be nickel(III) (in β-NiOOH form), according to diffraction peaks for (001) and (002) crystal faces at 19° and 37°.[39] It is noted that the peaks associated with $Ni(OH)_2$ disappeared after synthesis. The differences in peak intensities between spectra 2 and 3 could be explained by some differences in crystallinity (a slight amorphous phase could be present in sample 2) which could broaden the diffraction peaks.

Scanning electron microscopy (SEM) images were obtained using a microscope (JSM 7100F, JEOL®, Benelux) operated at 10 kV. As shown in Figure S5, the morphology of the various particles did not significantly change after the reaction with hypochlorite and the resulting particles could be assumed as spherical in shape with a wide size distribution from 1 to 30 µm.

A laser diffraction particle size analyzer (Mastersizer MS3000, Malvern Instruments®, UK) was used to determine the particle size distributions in terms of number and volume. The characteristic diameters of the number and volume distributions of the initial and synthesized powders are reported in Table 1. It should be noted that a slight growth in particle size occurs during synthesis, that is, the reaction with hypochlorite (mean value—sample 1: +26% and sample 2: +10%).

Relative densities of the nickel particles were measured via a helium pycnometer (AccuPyc 1330, Micromeritics®, USA). They underwent minor modifications both before and after the synthesis (refer to Table 1).

BET measurements (BELSORP-mini II, BEL®, Japan) were made to quantify the porosity and specific area of the particles. Since the synthesis reaction of nickel(III) particles consisted in exchanging an electron and a proton, the properties of the particles (porosity, pore diameter, and particle size) were slightly modified before and after synthesis. Table 1 summarizes all the physical properties of the initial nickel(II) powder and of the synthesized nickel(III) powders.

These measurements allow us to estimate the number of active sites on the two synthesized powders at 5.2×10^{22} and 1.9×10^{22} atoms per gram of powder, respectively for samples 1 and 2 according to Equation (10).

$$\frac{sites_{Ni^{(III)}}}{m_{cat}} = \frac{purity \times \mathcal{N}_A}{M_{NiOOH}} \quad (10)$$

where m_{cat} is the mass of powders (g), $\mathcal{N}_A$ is the Avogadro number (mol^{-1}), and M_{NiOOH} is the molar mass of NiOOH (g mol^{-1}).

2.2 | Kinetics investigations of the reaction between urea and chemically synthesized nickel(III) sites in alkaline medium

2.2.1 | Experimental set-up and reaction monitoring

The experimental set-up used to monitor the catalytic oxidation of urea by nickel(III) particles in an alkaline medium, consisted of a closed double-walled thermoregulated reactor operating in a nitrogen atmosphere (nitrogen was previously humidified to avoid any decrease in

TABLE 1 Physical properties of the initial nickel(II) powder and of the nickel(III) powders.

	Purity of nickel(III) content (%)	Density (g cm^{-3})	Particle size analysis (μm)										Specific surface area (m^2 g^{-1})	Mean pore diameter (nm)
			Volume distribution					Number distribution						
			d_{10}	d_{50}	d_{90}	d_{32}	d_{43}	d_{10}	d_{50}	d_{90}	d_{32}	d_{43}		
Initial Ni(II) powder	0	3.7 ± 0.1	3.9	9.0	16.9	5.4	9.8	0.4	0.5	0.8	5.5	10.0	6.67 ± 0.17	8.2 ± 0.1
Ni(III) powder—sample 1	79 ± 2	3.9 ± 0.1	5.5	12.3	24.0	9.9	13.7	1.3	3.4	8.1	9.9	13.7		
Ni(III) powder—sample 2	29 ± 2	3.8 ± 0.1	4.5	10.0	20.5	7.9	11.4	0.7	1.3	5.3	7.9	11.4	8.51 ± 0.12	7.7 ± 0.1

the reaction volume) (illustrated in Section S3, refer to Figure S6). The reactor initially contained a suspension of 5 g of synthesized powder in 45 mL volume of KOH solution for different concentrations. Ultrapure water 18.2 MΩ cm was systematically used to prepare suspensions. A strong stirring created by a suitable magnetic bar ($\frac{\phi_{\text{reactor}}}{\phi_{\text{magnetic bar}}} = \frac{6.5}{4.8}$, 800 rpm) ensured that all of the particles were thoroughly suspended. Before introducing urea, the suspension containing the NiOOH/Ni(OH)$_2$ particles was stirred for 5 min in order to finely disperse the nickel powder into the entire KOH volume. The aqueous deaerated alkaline solution of urea was then injected with a syringe through a septum. Each experiment was performed twice to ensure repeatability. pH was measured to identify the hydroxide ion consumption in order to study the reaction kinetics. To succeed, this method required a precise pH meter (three digits), calibrated for the appropriate pH range (pH 13–14), and a glass electrode, resistant to the suspension media. To fill these conditions, a Metrohm® Unitrode electrode was used so that the pH could be recorded every 0.5 s with an accuracy of ±0.001 pH units. Typical examples of the temporal variation of pH recorded in this study are shown in Figure S7. One could observe that, at the beginning of the recording, a transitional stage occurred corresponding to the time required to reach the perfectly mixed state of the liquid–solid suspension, before injecting the urea alkaline solution (5 mL). The two curves plotted on this figure also highlight the satisfactory repeatability of the experiments when two different solutions of urea in hydroxide solutions were injected in two identical suspensions of nickel(III) particles.

To understand how the reagent concentrations could affect the oxidation kinetic, and subsequently to identify the relevant kinetic parameters, an experimental workplan was established. It allowed varying the hydroxide concentrations from 5×10^{-3} to 5×10^{-2} mol L^{-1} and the urea concentrations from 10^{-2} to 3×10^{-1} mol L^{-1} (note that the latter value corresponds to the order of magnitude of the urea concentration in human urine). The choice was made to study synthetic urea solutions with concentrations close to those found in human urine[40] allowing a rapid preliminary optimization of the system. In addition, the nickel(III) concentration was modified by working with both nickel(III) powders of different purities.

As a preliminary step, it was verified that (i) the chemical reaction that occurred when the alkaline urea solution was put into contact with chemically synthesized nickel(III) particles led to the productions of by-products in the liquid phase identical to those that took place on the bare nickel electrode, and (ii) the total organic carbon (TOC) concentration decreased during the reaction. For this purpose, the analytical procedure established in our previous study[30] was used, involving ionic chromatography and nonpurgeable organic carbon.

2.2.2 | Postprocessing of the temporal pH-curves

The instantaneous rate of the reaction described by Equation (2), expressed in mol$\left(\text{m}^3\,\text{g}_{\text{cat}}\,\text{s}\right)^{-1}$ and noted r_χ, was defined as the derivative of the extent of reaction, ξ, as a function of time, as shown in Equation (11).

$$r_\chi = -\frac{1}{m_{\text{cat}} \times V}\frac{d\xi}{dt} = -\frac{1}{m_{\text{cat}} \times V}\frac{dn_{\text{CO(NH}_2)_2}}{dt} = -\frac{1}{m_{\text{cat}} \times V \times \nu_{\text{Ni(III)}}}\frac{dn_{\text{Ni(III)}}}{dt} = -\frac{1}{m_{\text{cat}} \times \nu_{\text{OH}^-}}\frac{d[\text{OH}^-]}{dt} \tag{11}$$

where m_{cat} is the nickel(III) mass (expressed in grams of catalyst, g_{cat}), ν_i is the stochiometric coefficient of the reactant i in Equation (2), V is the reaction mixture volume (assuming the volume constant versus time, m^3) and $n_{\text{Ni(III)}}$ is the amount of nickel(III) sites into the solid particles of NiOOH/Ni(OH)$_2$ that were accessible to the reagents (urea and OH$^-$).

The kinetic law of the chemical reaction was assumed to obey Equation (12).

$$r_\chi = k_\chi \times \left[\text{CO(NH}_2)_2\right]^{\alpha_\chi} \times [\text{OH}^-]^{\beta_\chi} \times (\rho_{\text{cat}})^{\gamma_\chi} \tag{12}$$

where $\alpha_\chi, \beta_\chi, \gamma_\chi$ are the partial orders of the reaction, respectively related to urea, hydroxide, and chemically synthesized nickel(III) sites, k_χ is the reaction rate constant (mol$^{1-(\alpha_\chi+\beta_\chi)}$ $(\text{m}^3_{\text{bulk}})^{\alpha_\chi+\beta_\chi+\gamma_\chi-1}$ $\text{g}_{\text{cat}}^{-(1+\gamma_\chi)}$ s^{-1}) and ρ_{cat} is the mass concentration of nickel(III) per unit of volume (g_{cat} m^{-3}).

Despite the similarity in terms of by-products, the fundamental mechanisms underlying the urea degradation (in particular adsorption/desorption ones) were different, depending on whether the nickel(III) sites used was electrochemically generated or chemically synthesized. For this reason, distinct notations were used for the

kinetic law: r_{χ} for chemically synthesized sites (defined in Equation (12)) and $r_{E\chi}$ for electrogenerated sites.

The conversion rate of the HCR reaction, noted X, could be calculated from the pH measurements, according to Equation (13).

$$X(t) = 1 - \frac{10^{pH_{(t)}-14}}{10^{pH_{t=0}-14}} \quad (13)$$

The experimental curves, $pH_{(t)}$, were systematically smoothed using a polynomial of order 6 as the raw data were slightly noisy, mainly due to disturbances caused by the stirring and specifically by the flow of the solid particles across the pH electrode.

In this work, the initial reaction rates, r_{χ}^{0}, were determined for conversions never exceeding 5% of the initial hydroxide concentration, and calculated from the slope of the $pH_{(t)}$ curve measured some seconds after the urea injection. The time period considered to calculate theses slopes (typically between 5 and 50 s) slightly impacted the obtained valued, as shown in Table S2 (refer to Section S4).

2.3 | Kinetic investigations of the reaction between urea and the electrochemically generated nickel(III) sites in alkaline medium

2.3.1 | Experimental set-up

The same set-up as the one developed in our previous study[30] was used for determining the partial orders. The three-electrode cell was connected to a potentiostat (PGSTAT 128 N, Metrohm Autolab®, Switzerland), and consisted of:

- a rotating nickel disk (2 mm diameter) as the working electrode (WE),
- a Hg/HgO as the reference electrode (Origasens, Origalys®, France),
- a Pt foil (40 mm^2) as the counter-electrode (CE).

All trials were repeated three times and the potentials were reported versus Hg/HgO throughout the article. The temperature of the reaction medium was regulated by flowing a thermostatic solution in the double-jacketed electrochemical cell. Measurements were performed using various concentrations of urea and KOH and four different working electrode surfaces, ranging from 8.7 to 15.4 mm^2. The latter were elaborated by introducing a thin square shaft into a glass tube filled with alkaline resistant glue and then polished to obtain a smooth rectangular section of bare nickel with surface areas as mentioned above.

2.3.2 | Expression of reaction rate

The reaction rate of the HCR on electrogenerated nickel(III) sites, standardized by the electrode surface, is expressed in mol. $\left(m_{elec}^{2}\, m_{bulk}^{3}\, s\right)^{-1}$ and defined as the flux density of the superficial chemical reaction by Equation (14).

$$r_{E\chi} = k_{E\chi} \times \left[CO(NH_2)_2\right]_{(t)}^{\alpha_{E\chi}} \times \left[OH^-\right]_{(t)}^{\beta_{E\chi}} \times \left(S_{elec}\right)^{\gamma_{E\chi}} \quad (14)$$

where $k_{E\chi}$ as the reaction rate constant ($mol^{1-\left(\alpha_{E\chi}+\beta_{E\chi}\right)} \left(m_{elec}^{2}\right)^{-\left(1+\gamma_{E\chi}\right)} \left(m_{bulk}^{3}\right)^{\alpha_{E\chi}+\beta_{E\chi}-1} s^{-1}$), S_{elec} is the surface of the bare nickel electrode (m_{elec}^{2}) and $\alpha_{E\chi}, \beta_{E\chi}, \gamma_{E\chi}$ the partial orders of urea, hydroxide, and electrochemically generated nickel(III), respectively.

3 | RESULTS ON THE KINETIC OF THE CATALYTIC INDIRECT UREA OXIDATION

3.1 | Case 1: with chemically synthesized nickel(III) sites

3.1.1 | Determination of the initial kinetic rate law

The initial rate method is a well-known approach,[41,42] enabling the partial orders of each reactant to be determined by varying studied reactant concentration while keeping constant the other reactant concentrations and the operating conditions constant (temperature and stirring).

To determine the partial order of urea, noted α_{χ}, several temporal pH measurements were performed and the related initial rates, r_{χ}^{0}, determined. By varying the initial concentration of urea from 0.02 to 0.25 mol L^{-1}, and by keeping $[OH^-] = 0.005$ mol L^{-1} and the nickel particle mass equal to 30 $kg_{cat}\, m^{-3}$ (nickel(III) powder—sample 2), the initial kinetic rate law (Equation (11)) can be written as Equation (15).

$$r_{\chi}^{0} = k_{app} \times \left[CO(NH_2)_2\right]^{\alpha_{\chi}} \quad (15)$$

where k_{app} is the related apparent constant ($mol^{1-\alpha_{\chi}} \left(m_{bulk}^{3}\right)^{\alpha_{\chi}-1} \left(g_{cat}\, s\right)^{-1}$).

The variation of the logarithmic initial reaction rate versus the logarithmic urea concentration, plotted in Figure 1A, can be assumed linear despite a rather strong dispersion. From the slope of the related straight line, the partial order of urea is found equal to $\alpha_{\chi} = 0.2 \pm 0.1$. This low value suggests that the kinetic rate slightly depends on the urea concentration, which can be explained by these assumptions:

(i) the strong affinity of urea to the nickel peroxide particles. Several works have studied the adsorption of urea molecules on various adsorbents: nickel(II) oxide NiO,[43] nickel nanoparticles embedded in carbon nanotubes,[44] and nickel(III) sites.[45] Whatever the adsorbent nature, a strong affinity of urea with nickel[43] and a low adsorption energy of urea[46] have been reported. According to the Langmuir isotherm theory (Equation (16)), the adsorbate forms a single layer onto an adsorbent surface.[47] The adsorbate (urea) amount can be expressed using the equilibrium constant of the adsorption step, K, and the maximum nickel(III) surface concentration, Γ_{max} (mol m^{-2}). It is important to keep in mind that a multilayer urea adsorption on the active nickel(III) sites seems hard to

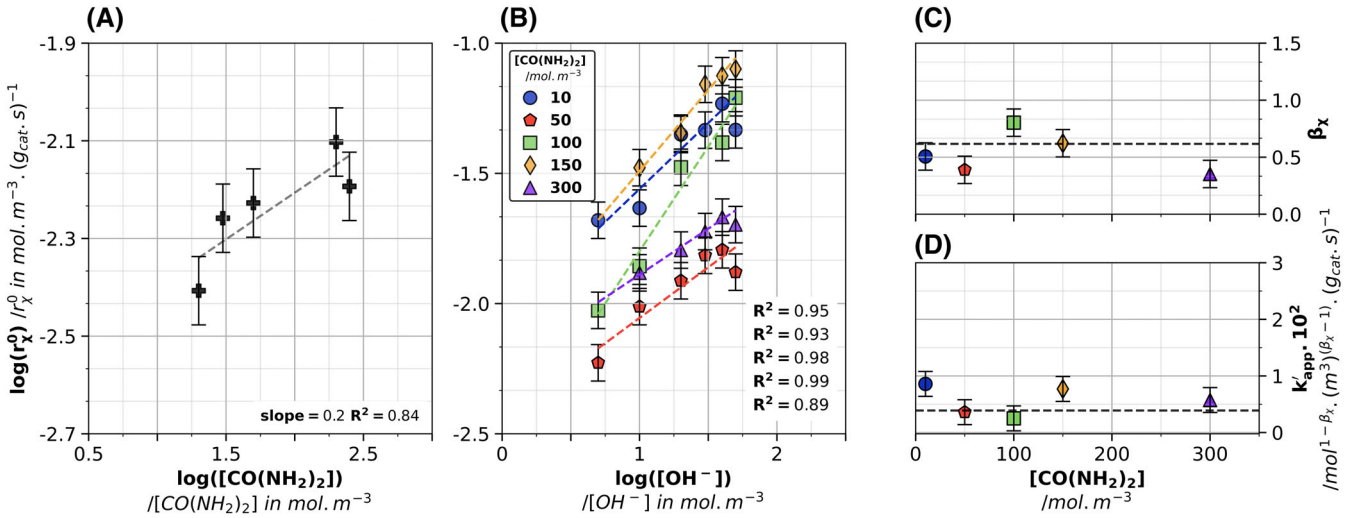

FIGURE 1 Kinetic experiments with chemically synthesized nickel(III) sites: measurements of the initial rate versus the concentration of (A) urea and (B) potassium hydroxide. Graph (C) provides the values of β_χ as a function of the KOH concentration for different urea concentrations. k'_{app} remains constant whatever the urea concentration, as shown in the graph (D). Graph (A) was achieved with a 5 mmol L^{-1} KOH solution. All these results were obtained with nickel(III) synthesized powder—sample 2.

envisage due to the steric effects and to the weak affinity of oxygen to nitrogen.

$$\Gamma = \frac{\Gamma_{max} \times K \times [CO(NH_2)_2]}{1 + K \times [CO(NH_2)_2]} \quad (16)$$

where Γ the nickel surface concentration (mol m^{-2}).

In this case, the urea superficial concentration on the nickel(III) sites can be simplified ($K \times [CO(NH_2)_2] \gg 1$) as Equation (17).

$$\Gamma = \Gamma_{max} \quad (17)$$

This means that adsorption is rapid and limited by accessible nickel(III) sites. Once one urea reacts with two nickel(III) sites, the intermediates must desorb and subsequently compete with urea for adsorption on the active sites. The urea concentration remains lower than the amount of nickel(III) sites.

(ii) the mass transfer limitations of the reagents into the internal nickel oxides layers of core–shell particles.[48]

The same method was implemented for determining the hydroxide partial order, β_χ, by varying the related concentration between 0.005 and 0.05 mol L^{-1}. Here, the simplified initial kinetic rate law can be deduced from Equation (11) and can be written as Equation (18).

$$r^0_\chi = k'_{app} \times [OH^-]^{\beta_\chi} \quad (18)$$

where k'_{app} is the related apparent constant (as $k'_{app} = k_\chi \times [CO(NH_2)_2]^{0.2} \times (\rho_{cat})^{\gamma_\chi}$).

Figure 1B presents the variation of the logarithmic initial reaction rate versus the logarithm of the hydroxide concentration, for five different urea concentrations ranging from 0.01 to 0.3 mol L^{-1}. These variations are assumed linear and their slopes, determined for various urea concentrations, are reported in Figure 1C. This leads to $\beta_\chi = 0.6 \pm 0.2$. As urea has been found to slightly impact the reaction rate, a small variation of the apparent constants, k'_{app}, as a function of the urea concentration is observed in the inset of Figure 1D, likely due to some measurement errors. From this, an average value of the apparent constant is found equal to 0.38×10^{-2} $mol^{0.4}$ $(m^3_{bulk})^{-0.4}$ $(g_{cat}\,s)^{-1}$.

By modifying the nickel(III) purity of the synthesized powders (samples 1 and 2, refer to Table 1) and keeping constant the initial concentrations of urea at 0.3 mol L^{-1} and of hydroxide at 0.005 mol L^{-1}, the partial order of nickel(III), γ_χ, can be deduced as Equation (19).

$$r^0_\chi = k''_{app} \times (\rho_{cat})^{\gamma_\chi} \quad (19)$$

where k''_{app} is the related apparent constant (mol $(m^3_{bulk})^{\gamma_\chi - 1}$ $g_{cat}^{-(1+\gamma_\chi)}$ s^{-1}).

Considering that the mass concentration of nickel(III), ρ_{cat}, is the product of the mass of powder introduced and the nickel(III) content in the powder, the slope of Equation (20) allows the reaction order of nickel(III) to be determined.

$$\ln\left(r^0_\chi\right) = \ln\left(k''_{app}\right) + \gamma_\chi \times \ln(\text{mass of powder} \times \text{purity}) \quad (20)$$

Finally, γ_χ is found almost equal to 1.9 ± 0.2 which can be interpreted as the number of nickel(III) sites (NiOOH in fact) involved in the urea oxidation reaction.

Once the partial orders are determined, the kinetic constant, k_χ, is calculated using the values of (i) initial concentrations of the reagents and of (ii) initial rates measured for 35 trials according to Equation (12). As illustrated in Figure S8 (refer to Section S5), k_χ ranges from $k_{\chi,low} = 0.24 \times 10^{-12}$ to $k_{\chi,high} = 7.7 \times 10^{-12}\ mol^{0.2}\ (m^3_{bulk})^{1.7}\ g_{cat}^{-2.9}\ s^{-1}$, and the average value equal to is $k_{\chi,mean} = 3.8 \times 10^{-12}\ mol^{0.2}\ (m^3_{bulk})^{1.7}\ g_{cat}^{-2.9}\ s^{-1}$.

Therefore, the overall empirical kinetic law of urea oxidation in presence of chemically generated nickel(III) sites can be expressed by Equation (21).

$$r_\chi = (3.8 \pm 2.0) \times 10^{-12} \times \left[CO(NH_2)_2\right]^{0.2} \times [OH^-]^{0.6} \times \rho_{cat}^{1.9} \quad (21)$$

It should be kept in mind that (i) as the urea molecules penetrate into the NiOOH/$Ni(OH)_2$ particles, they are oxidized and the NiOOH is reduced to $Ni(OH)_2$ and (ii) the urea oxidation products generated then have to diffuse deeper into the particle to encounter another nickel(III) active site and to continue their mineralization. As mentioned above, the occurrence of mass transfer limitations could also contribute to slowing down the reaction rate.

In the case of such synthesized nickel particles, the regeneration of nickel(III) sites cannot occur after being consumed by urea; the UEO by-products must desorb and meet another new nickel(III) site, introducing possible additional mass transport limitation phenomena.

3.1.2 | Validation of the initial kinetic rate law by the integral method

In this section, it is assumed that there is no limitation by the mass transport (urea or/and OH^-), inside or outside of the NiOOH/Ni$(OH)_2$ particles. Following this assumption, the validity of the kinetic rate law determined previously (Equation (21)) must be confirmed. To this end, it is necessary to numerically integrate the equation as a function of time and to confront the theoretical temporal evolutions of the reactant concentrations with the experimental data.

Using the integral method for kinetic investigations offers the advantage[49] to validate the reaction orders and the rate constant value obtained using the initial rate method (i.e., at short times and very low OH^- conversions below 5%) for longer periods where high conversions are achieved and where secondary reactions can also occur. The method for doing so entails a comparison between the experimental and predicted temporal variations in OH^- concentration in order to validate the law derived from initial kinetics.

Table 2 presents the chemical amounts of reactants, initially and at any time, where X represents the hydroxide conversion rate.

Without considering the real accessibility of the nickel(III) sites in the synthesized core–shell particles, the theoretical profiles tend toward the experimental values but significant deviations of magnitude are obtained (deviation > 50%) and are even greater for the highest reactant concentration (results not shown).

In order to describe the physics of the system (i.e., spherical layers of NiOOH around a core of $Ni(OH)_2$), a surface accessibility factor of nickel(III), noted ε, is voluntarily introduced. Such choice is motivated by the fact that (i) the spatial distribution of nickel(III) on solid particles is probably not uniform, and (ii) the oxidation reaction of urea on nickel particles is a surface reaction, and the by-products and reaction intermediates formed inside the particle consume the OH^- ions. This latter consumption, not considered in the kinetic model studied here, will lead to a diffusional limitation of hydroxide ions within the particles. The parameter, ε, offers the advantage to fill this bias. Note that the relating value, not measured, will be the single fitting parameter of the model.

By coupling Equation (11) expressed as a function of hydroxide ions and Equations (21) and (22) is obtained.

$$\frac{dX}{dt} = \frac{6 m_{cat} k_\chi b^{0.6}}{[OH^-]^0} \times \left(\frac{6a - bX}{6V}\right)^{0.2} \times \left(\frac{(1-X)}{V}\right)^{0.6} \times \left(\frac{(c' - bX) \times M_{NiOOH}}{V}\right)^{1.9} \quad (22)$$

The previous equation is numerically solved (using scipy.integrate.odeint Python package solving a system of ordinary differential equations), and the theoretical temporal conversion of hydroxide with time is obtained, as reported in Figure 2. The surface accessibility factor of nickel(III), ε, used to plot these figures is equal to 2.6%, suggesting then that a small amount of nickel(III) is available for the chemical reaction. Indeed, after a first cycle of adsorption, the urea molecules having a strong affinity to nickel(III) could induce a "screen effect", thus reducing the number of nickel(III) sites into the internal layers of the particles. Figure 2 also reports a sensitivity study with regard to the chemical kinetic constant, k_χ: a maximum deviation of 20% is observed for the reaction times longer than 600 s. The validity of the kinetic rate law is then checked by considering several initial concentrations of urea and hydroxide ions. Whatever the concentrations, the numerical profiles of the conversion of OH^- do not deviate (maximum deviation of 6%) from the experimental data for $X < 20\%$ ($\varepsilon = 2.6\%$). As expected, higher conversions are observed when the initial hydroxide ions' concentration is decreased.

Figure 2 shows that the temporal profiles obtained using the kinetic rate law constant $k_{\chi,low}$, $k_{\chi,mean}$ or $k_{\chi,high}$ determined from the previous section (refer to Section S5) correlate very well (maximum deviations of 10%) with the experimental ones for a period longer than 200 s. It can be noted that for unfavorable conditions, illustrated in Figure 2C (i.e., the lowest ratio between the initial concentration of hydroxide ions and urea, almost equal to 1.7×10^{-2}), the deviation between the experimental and predictive profiles is higher than 20% after 600 s. This slowing down of the urea oxidation could be explained by two assumptions: (i) an internal diffusional limitation of the reactants (urea and hydroxide) and by-products in the particles could limit the reaction process after consuming all the nickel(III) active sites on the catalyst surface and (ii) a competitive adsorption between the by-products and the reactants could also occur.

	Moles of $CO(NH_2)_2$	Moles of OH^-	Moles of NiOOH	Moles of accessible NiOOH
$t = 0$	$a = [CO(NH_2)_2]^\circ V$	$b = [OH^-]^\circ V$	$c = \frac{m_{cat}}{M_{NiOOH}} \times$ purity	$c' = c \times \varepsilon$
t	$a - \frac{bX}{6}$	$b(1-X)$	$c - bX$	$c' - bX$

Note: V represents the liquid reaction volume (4.5×10^{-5} m^3), m_{cat} is the mass of powder (5 g), M_{NiOOH} is the NiOOH molar mass (91.7 g mol^{-1}) and X is the conversion in hydroxide ions. The corresponding overall reaction is written as $CO(NH_2)_2 + 6OH^- + 6Ni^{+III} \rightarrow$ Products.

TABLE 2 Extent of urea oxidation reaction by chemically synthesized nickel(III) sites.

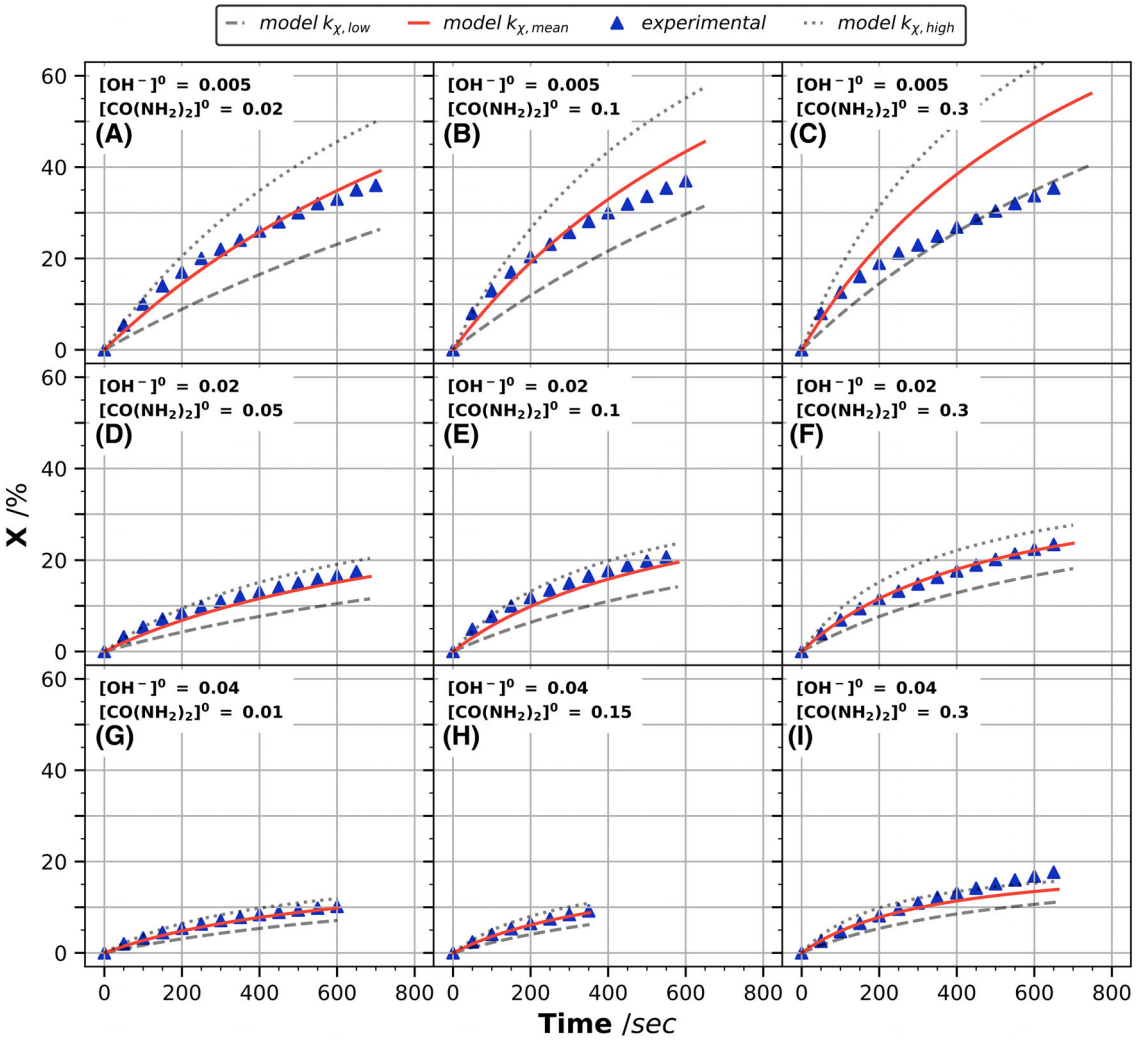

FIGURE 2 Comparison of the experimental temporal evolutions of the hydroxide ion conversion to the ones obtained by numerical solving of Equation (22) for different initial concentrations of urea and hydroxide (molar concentration are expressed in mol L^{-1}). The surface accessibility factor of nickel(III), ε, is equal to 2.6% whatever the graphs.

3.2 | Case 2: with the electrochemically synthesized nickel(III) sites on bare nickel electrode

In the present section, the NiOOH sites are electrochemically regenerated on a bare nickel anode and react with urea. As shown in our previous work,[30] the coupling of the HCR (urea/NiOOH) with the ER ($NiOOH/Ni(OH)_2$) allows the continual regeneration of the active nickel(III) sites if the nickel oxide anode is polarized to the appropriated potential. It becomes then possible to study only the HCR and thus to avoid the adsorption/desorption processes as well as the mass transport of urea and oxidation products from one nickel(III) molecule to the other (refer to Section 3.1.2). For that, the current potential curves have been plotted by applying a potential scan rate lower than 1 mV s^{-1}. This technique has been applied here for different operating parameters, with the aim of establishing the kinetic law of the UEO in presence of electrogenerated NiOOH sites at the anode.

The *i*–*E* curves obtained at steady state conditions are showed in Figure 3A–C. From them, the partial orders of urea, hydroxide ions

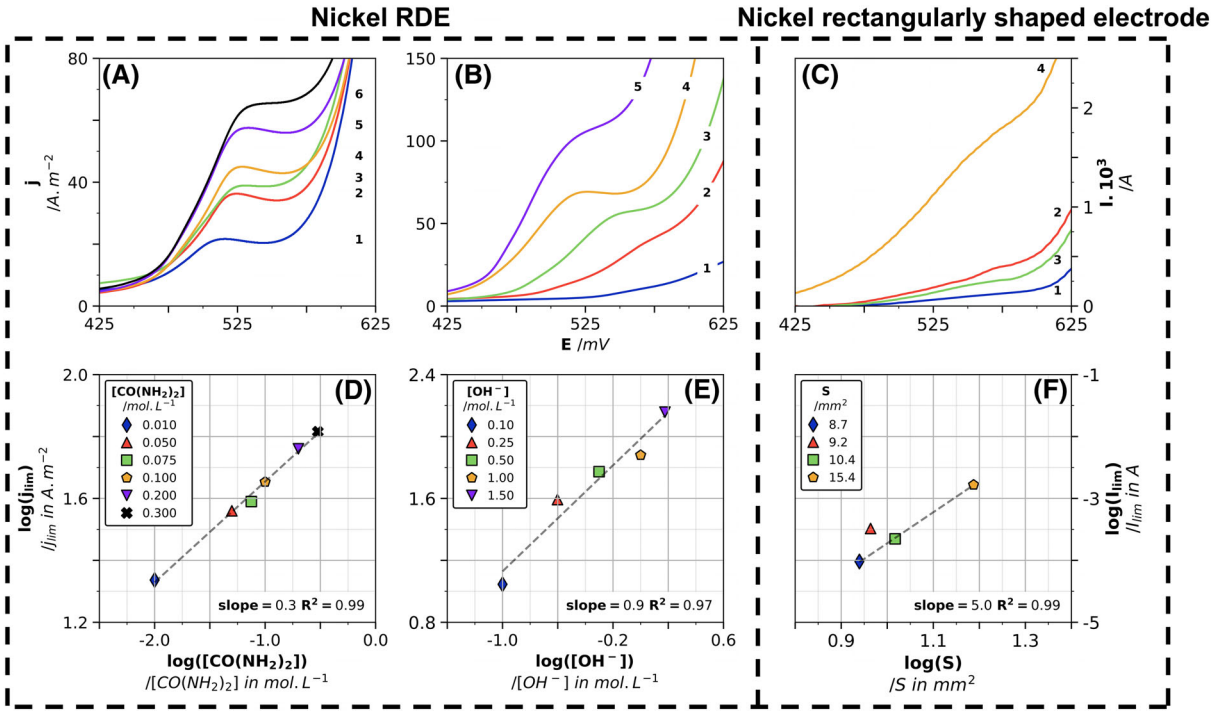

FIGURE 3 Kinetic experiments with electrochemically synthesized nickel(III) sites on bare nickel electrode. Graphs (A)–(C) present *j*/*i*–*E* curves obtained at the steady state (0.12 mV s^{-1}) using a Ni WE immersed in 100 mL of alkaline solutions of urea, thermoregulated at 298 K. Graph (A) effect of urea concentration on the shape of the *i*–*E* curves obtained on nickel RDE in alkaline solution of KOH (1 mol L^{-1}) at 1000 rpm with urea concentrations at 0.01 mol L^{-1} (1), 0.05 mol L^{-1} (2), 0.075 mol L^{-1} (3), 0.1 mol L^{-1} (4), 0.2 mol L^{-1} (5) and 0.3 mol L^{-1} (6). Graph (B) effect of KOH concentration on the shape of the *i*–*E* curves obtained on nickel RDE in urea solution of 0.3 mol L^{-1} stirred at 1000 rpm with hydroxide concentrations at 0.1 mol L^{-1} (1), 0.25 mol L^{-1} (2), 0.5 mol L^{-1} (3), 1 mol L^{-1} (4) and 1.5 mol L^{-1} (5). Graph (C) effect of the geometric surface area (rectangularly area) of the nickel electrode on the shape of the *i*–*E* curves obtained with a urea concentration of 0.3 mol L^{-1} and a KOH concentration of 1 mol L^{-1}, using geometrical electrode surfaces equal to 8.7 mm^2 (1), 9.2 mm^2 (2), 10.4 mm^2 (3) and 15.4 mm^2 (4). The partial orders of urea ($\alpha_{E,\chi}$), hydroxide ions ($\beta_{E,\chi}$) and nickel(III) ($\gamma_{E,\chi}$) were determined from the curves respectively plotted in figures (D)–(F), deduced from the logarithm plot of the limiting current magnitude (at the diffusion limitation area) as a function of the logarithmic reactant concentration.

and nickel(III) sites have been determined, as shown in Figure 3D–F respectively.

The potentiostatic polarization of the nickel electrode at the plateau of the *i*–*E* curves allows the anode to be covered by $Ni(OH)_2$ which oxidizes into NiOOH. The urea is oxidized by a chemical reaction with NiOOH which is reduced into $Ni(OH)_2$, immediately oxidized on the nickel electrode into NiOOH, thus releasing its electron. The newly regenerated NiOOH goes on a new cycle with the urea oxidation intermediate, thus meaning that the urea and its by-products formed could be oxidized by the same nickel system, without any mass transfer limitation. The oxidation process continues until obtaining the final products (N_2, CO_2, etc.).

Under steady state conditions, the mass balance on nickel(III) is expressed as Equation (23).

$$\frac{d\Gamma_{III}}{dt} = \frac{I_{plateau}}{n\mathcal{F}S_{electrode}} - \nu_{Ni^{III}} \times r_{E\chi} \times V \tag{23}$$

where Γ_{III} is the nickel surface concentration (mol m^{-2}), $I_{plateau}$ as the limiting current, observed at the plateau signal (A), *n* is the number of exchanged electron (1, dimensionless), $\mathcal{F}$ the Faraday constant (C mol^{-1}), $\nu_{Ni^{III}}$ the stoichiometric coefficient of nickel(III) and $r_{E\chi}$ is the reaction rate of the HCR on electrogenerated nickel(III) sites (mol $\left(m^2_{elec}\, m^3_{bulk}\, s\right)^{-1}$).

It is obvious that after a certain time, the redox system NiOOH/$Ni(OH)_2$ will reach a steady state until the concentration of urea is sufficient to supply the system. In this case, the accumulation of the nickel(III) at the nickel surface can be assumed equal to zero. The current intensity of the plateau is thus proportional to the reaction rate as Equation (24).

$$I^{\infty}_{plateau} = n\mathcal{F} \times V \times \nu_{Ni^{III}} \times k_{E\chi} \times \left[CO(NH_2)_2\right]^{\alpha_{E\chi}} \times [OH^-]^{\beta_{E\chi}} \times \left(S_{electrode}\right)^{\gamma_{E\chi}+1} \tag{24}$$

where $I^{\infty}_{plateau}$ is the limiting current in steady state conditions (A).

As for the initial rate method in Section 3.1.1, by applying the logarithm to Equation (24) and by varying the molar concentration of one reactant, the partial orders can be deduced, according to Equations (25)–(27).

$$\log\left(j^{\infty}_{plateau}\right) = \log\left(n\mathcal{F} \times k_{E\chi} \times [OH^-]^{\beta_{E\chi}} \times \left(S_{electrode}\right)^{\gamma_{E\chi}}\right) + \alpha_{E\chi} \times \log\left(\left[CO(NH_2)_2\right]\right) \tag{25}$$

$$\log\left(j^{\infty}_{\text{plateau}}\right) = \log\left(n\mathcal{F} \times k_{E\chi} \times \left[CO(NH_2)_2\right]^{\alpha_{E\chi}} \times \left(S_{\text{electrode}}\right)^{\gamma_{E\chi}}\right) + \beta_{E\chi} \times \log([OH^-]) \quad (26)$$

$$\log\left(I^{\infty}_{\text{plateau}}\right) = \log\left(n\mathcal{F}S_{\text{electrode}} \times k_{E\chi} \times \left[CO(NH_2)_2\right]^{\alpha_{E\chi}} \times [OH^-]^{\beta_{E\chi}}\right) + \gamma_{E\chi} \times \log\left(S_{\text{electrode}}\right) \quad (27)$$

where $j^{\infty}_{\text{plateau}}$ is the limiting current density corresponding to the plateau of the signal in steady state ($A\,m^{-2}$).

The related plots are reported in Figure 3D–F. A value of $\alpha_{E\chi} = 0.3 \pm 0.1$ is obtained for the partial order of urea, which correlates to the value obtained with chemically synthesized nickel(III) sites (refer to Section 3.1.1). The partial order of hydroxide ions is found equal to $\beta_{E\chi} = 0.9 \pm 0.1$. This value is slightly higher than the previous one ($\beta_{\chi} = 0.6$), which can be attributed to the fact that in addition to urea oxidation, the electrogeneration of nickel(III) requires one hydroxide ion and thus implies a stronger dependence on the chemical rate by hydroxide ions. Lastly, the partial order of nickel(III) is found equal to $\gamma_{E\chi} = 5.0 \pm 0.5$. This high value would suggest that, during the potentiostatic polarization, a nickel active site is regenerated five times on the electrode surface per adsorbed urea. Since the number of urea adsorption sites onto nickel(III) is continuously electrogenerated, the adsorbed urea molecule can be completely oxidized without any desorption of intermediates, contrary to the case with chemically synthesized particles, containing sacrificial NiOOH.

Once the partial orders are known, the kinetic constant, noted $k_{E\chi}$, is deduced using the same method as in Section 3.1.1. On the basis of 11 experiments carried out (refer to Section S6), $k_{E\chi}$ is found to vary in the range from 2.32×10^{24} to $4.24 \times 10^{24}\,mol^{-0.2}\,(m^2_{elec})^{-6}\,(m^3_{bulk})^{0.2}\,s^{-1}$. The average value is equal to $2.86 \times 10^{24}\,mol^{-0.2}\,(m^2_{elec})^{-6}\,(m^3_{bulk})^{0.2}\,s^{-1}$ and used for the following calculations. The magnitude of this apparent constant reflects the heterogeneous nature of the HCR reaction. Indeed, the value of the apparent constant is issued from a kinetic law which involves, on the one hand, volume concentrations and, on the other, a superficial concentration (normalized to the catalyst mass for r_{χ}) at a high partial order (2 for r_{χ} and 5 for $r_{E\chi}$).

Finally, the proposed kinetic law for the urea oxidation by the electrochemically generated nickel(III) sites can be written as Equation (28).

$$r_{E\chi} = (2.86 \pm 1.38) \times 10^{24} \times \left[CO(NH_2)_2\right]^{0.3} \times [OH^-]^{0.9} \times \left(S_{\text{electrode}}\right)^5 \quad (28)$$

3.3 | Proposed mechanism for the complete urea electrooxidation

Based on previous work,[30] Figure 4A,B proposes an overall mechanism for urea degradation involving electrochemically generated nickel(III) sites. The reaction scheme is composed of different pathways leading to the formation of by-products previously identified in the liquid phase.

The urea degradation mechanism from electrogenerated nickel(III) site can be classified into the nucleophilic oxidation reaction class[50,51] (as for the methanol oxidation on nickel(III)[52]), involving two pathways successively: (i) electrogenerated $Ni(OH)_2$ catalyst dehydrogenation reaction followed by (ii) a spontaneous nucleophilic dehydrogenation reaction. First, the urea is adsorbed on a nickel(III) site,[53] formed by the catalyst dehydrogenation reaction of nickel(II) oxidation. By analogy to the urease action on urea,[54,55] a second active nickel(III) site is required to pursue oxidation (step 2). Following the first nucleophilic attack on a hydroxide group, two reactional pathways (step 3 and/or step 20) can be considered, favoring the formation of either ammonia (step 5), nitrite (steps 4, 8–19), carbonate ions (steps 4–7), or cyanate ions (steps 20–22). The formation of ammonia and carbonate ions belongs to the same reactional pathway, thus suggesting an equimolar formation of these by-products over time. The nitrification route on nickel sites shown in Figure 4B leads to the formation of nitrite. This route has been already studied by DFT,[56] voltammetry and electrolyzes.[57] This latter route does not rule out the production of nitrogen during oxidation, even if several works[24,25,30,58] have reported the overoxidation of nitrogen into undesired NOx compounds at the expense of a nitrogen production. It should be noted that (i) the formation of cyanate (steps 21–22) and nitrite (steps 4, 18, 19) ions occurs in equimolar condition, and (ii) most of the reactions constituting the proposed mechanism require hydroxide ions, and consequently directly decrease the local pH at the electrode surface. The proposed mechanism illustrates a succession of redox reactions between the catalyst (i.e., nickel(III)), both adsorbed urea and oxidation intermediates. The main idea of this mechanism is that nickel(II) is continuously oxidized into nickel(III) at the applied potential, thus providing a continuous source of electrons for UEO. Note that Wang et al.[31] summarized various mechanism found in the bibliography without any quantitative mass balances after electrolyzes. These works consider that the attack of hydroxide ions (strongly alkaline electrolyte) allows deprotonation of adsorbed urea. In the future, one can expect that using ad hoc co-catalysts, or even fine controlled potential would make it possible to favor certain mechanistic pathways so as to increase, for example, the yield of nitrogen to the detriment of the nitrite production.[14,59]

This reaction scheme reflects the complexity of a fully detailed kinetic approach that will require a very large number of experiments so as to be able to determine each elementary kinetic constant (from k_1 to k_{22}, forward and backward).

4 | GLOBAL MODELING OF THE UREA ELECTROOXIDATION

4.1 | Establishment of the predictive model

Various potentiostatic electrolyzes with high conversions of urea have been performed in our previous work,[30] for which the variations of the concentrations of urea and by-products with electrolyzes times have been determined and can be thus used to validate the model. The latter is based on the kinetic data obtained in the previous sections and involves all the physical processes occurring at the anode

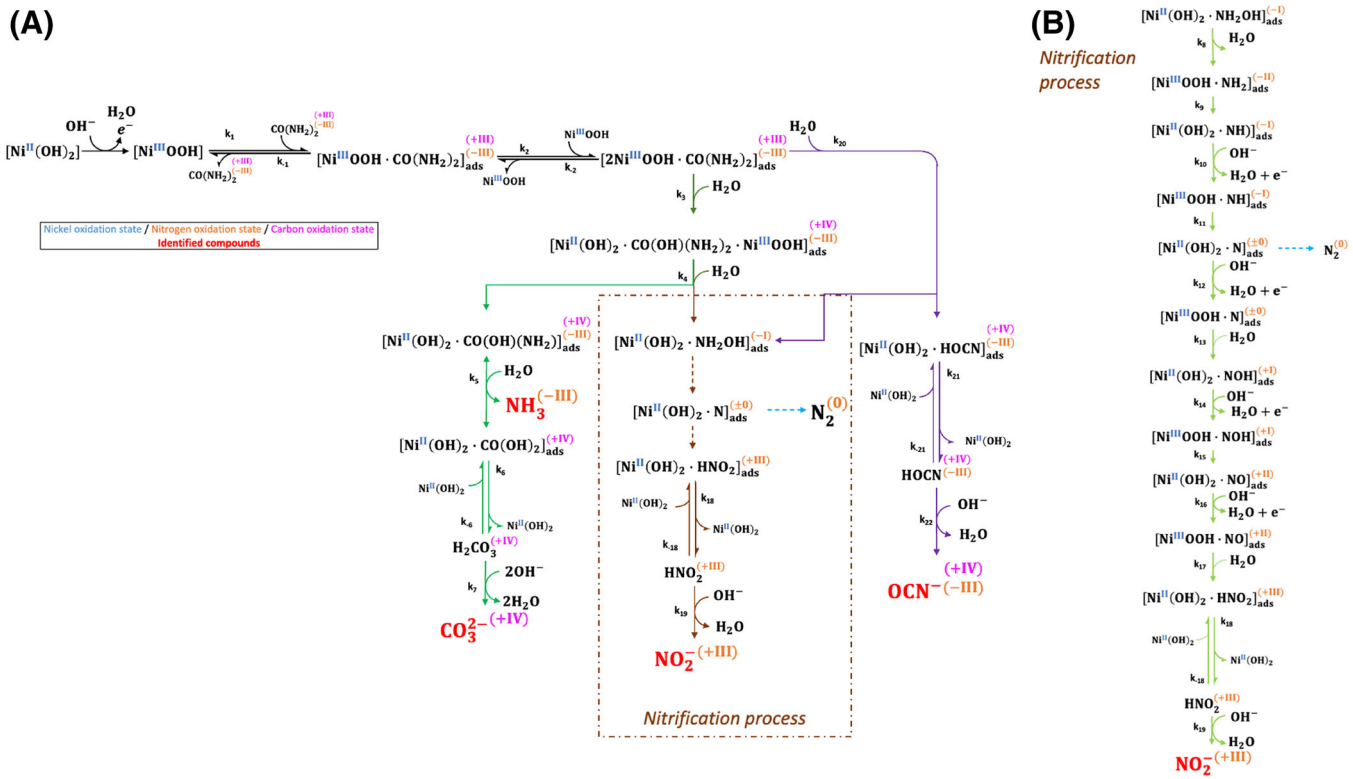

FIGURE 4 Proposed overall mechanism for UEO in alkaline media on a bare nickel anode covered after polarization by the system NiOOH/Ni$(OH)_2$. On the left side, (a) the mechanism shows the main and side chemical pathways leading to N_2 and CO_2 (under CO_3^{2-} form) as well as the by-products previously identified in the liquid phase[30] and (b) detailed nitrification route.

and in the bulk. Besides, the model is expected to be applicable on a large scale.

A one-dimensional description, as a function of the distance to the electrode, can be considered sufficient (for parallelepipedal electrochemical cells and planar anodes) to solve the mass transport phenomena coupled to the HCR in a porous catalytic layer. A schematic representation of the half-cell is given in Figure 5.

The aim here is to model the behavior of the electrochemical system during potentiostatic electrolyzes on a massive nickel electrode (supposed in equipotential conditions) of a stirred aqueous solution of urea in an alkaline medium. During the electrode polarization, the following reactions will take place on the nickel compounds; starting with Equation (29) and followed by Equation (1). At the applied electrolyzes potential (i.e., the one measured at the diffusion plateau of *i*–*E* curves, 0.55 V as illustrated in Figure 3), the reaction described in Equation (29) occurs until the electrode is completely covered by a Ni$(OH)_2$ layer. Then the catalytic cycle urea/NiOOH/Ni$(OH)_2$ occurs.

$$Ni + 2OH^- \rightarrow Ni(OH)_2 + 2e^- \quad (29)$$

4.1.1 | Model assumptions

With the objective of building a robust model, it is necessary to formulate a clear framework and the appropriated assumptions:

(i) Nickel(II) oxidation reaction occurs in a layer of a constant thickness μ which porosity ω, tortuosity τ and surface in contact with the solution remain unchanged throughout the electrolysis. Such assumption is supported by the fact that no significant release of nickel oxides has been measured by inductively coupled plasma (ICP) measurements performed at the end of each electrolysis (detection limit equals 100 ppb). Porosity is evaluated considering that the nickel sites in the reactive layer are disposed as face-centered cubic unit cell with an atomic packing factor estimated at 0.74. Moreover, the tortuosity, τ, is estimated at $\pi/2$ as the ratio between the half-circumference of a sphere ($\pi \times r$) and the diameter of the sphere ($2 \times r$) (corresponding to the shortest path). The diffusion coefficient in the reactive layer ($\delta < z < \delta + \mu$) is then calculated as an effective diffusion coefficient $D_{i,w}^{eff}$ according to Equation (30).

$$D_{i,w}^{eff} = D_{i,w} \times \frac{\omega}{\tau} \quad (30)$$

where $D_{i,w}$ is the diffusion binary coefficient of the specie *i* in the water ($m^2\,s^{-1}$), ω is the porosity of the layer of thickness μ (dimensionless), and τ the tortuosity (dimensionless).

The values of the urea diffusion coefficient were previously calculated for different KOH concentrations, from the Stokes–Einstein equation.[30]

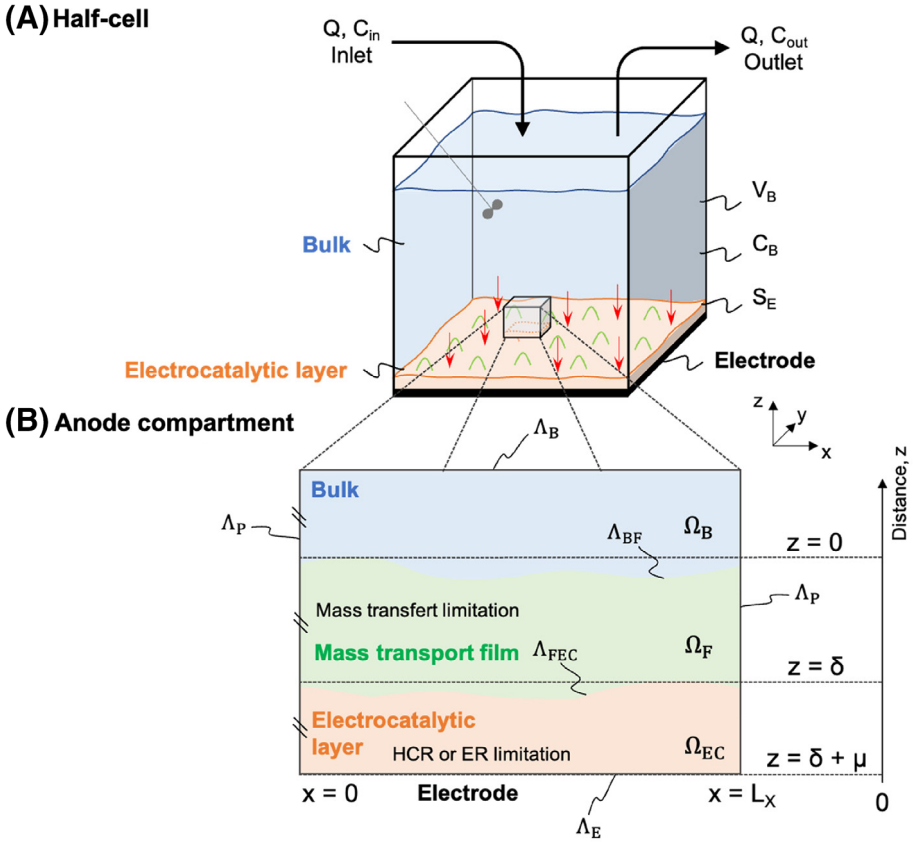

FIGURE 5 (A) Schematic representation of the electrochemical half-cell. The large scale includes a perfectly stirred liquid phase and an electroactive layer of nickel oxide mixtures on the metal electrode surface. (B) View of the various sensitive areas including possible limiting physical phenomena. The enlargement scheme contains three subdomains characterized by the occurrence of different phenomena: (1) a perfectly mixed zone, Ω_B, that is connected to the bulk liquid, (2) a mass transport boundary film Ω_F, and (3) the matrix of the electrocatalytic nickel oxide layer Ω_{EC} at the electrode surface. Each boundary of the system is labeled by Λ. Λ_{BF} represents the boundary between the bulk Ω_B and mass transport boundary film Ω_{EC} areas. Λ_{FEC} represents the boundary between the film Ω_F and electrocatalytic film Ω_{EC} areas. Λ_E and Λ_B represent the massive electrode and wall boundaries of the system, respectively (illustration adapted from Picioreanu et al.[68]).

(ii) The nickel oxides $Ni(OH)_2$ and NiOOH are considered here as electronic conductors,[60,61] making the electronic transfer invariant in the whole μ layer. Most of the electrolyzes are performed under potentiostatic conditions. Since the applied potential is sufficiently anodic to allow (energetically speaking) the immediate conversion of any $Ni(OH)_2$ released from the HCR to NiOOH, one can assume that after a few minutes' electrolysis, the surface concentrations of $Ni(OH)_2$ and NiOOH become constant and that the term related to the accumulation of these species is null. It is assumed that all the active sites in the reactive layer ($\delta < z < \delta + \mu$) are electronic conductors, in contact with the ions in solution. This hypothesis is supported by the following points:

- according to previous work,[30] one ER/HCR cycle occurs more than 100 times at low scan rates (i.e., <1 mV s^{-1}). The nickel(III) or nickel(II) cannot thus crystallize in an organized lattice, which creates some disorder in this layer.[22]
- moreover, at the initial time, the massive nickel electrode is only composed of nickel(0). As a result of polarization, the layer thickness grows toward the massive nickel(0) electrode: a previous study using *i*–*E* curves highlights that 110 layers of active sites are formed.[30] For forming a new layer, a hydroxide ion should be present and must diffuse/migrate from the bulk, according to Equation (1). The water molecules produced should also be removed from the layer by mass transport.

(iii) The geometry of the system is supposed to be independent of the length and width of the reactive layer and the radial diffusion to be negligible. Once formed, NiOOH will react with urea and hydroxide ions according to Equation (31).

$$r_{E\chi}(\delta \le z \le \delta+\mu, t) = k_{E\chi} \times [OH^-]^{\beta_{E\chi}} \times (S_{elec})^{\gamma_{E\chi}} \times \left[CO(NH_2)_2\right]^{\alpha_{E\chi}}_{(\delta \le z \le \delta+\mu, t)} = k_{app} \times \left[CO(NH_2)_2\right]^{\alpha_{E\chi}}_{(\delta \le z \le \delta+\mu, t)} \quad (31)$$

where k_{app} is the apparent constant ($mol^{1-\alpha_{E\chi}} (m^2_{elec})^{-1} (m^3_{bulk})^{\alpha_{E\chi}-1} s^{-1}$).

It should be noted that the proposed kinetic equation does not take into account the consumption of nickel peroxide and hydroxide ions during the chemical reactions leading to products and by-products.

(iv) The concentration of urea and hydroxide ions in the layer μ is considered as a spatially continuous function; the nickel particles are assumed to be small enough not to impact the spatial concentration profile.

4.1.2 | Governing equations: urea mass balances

From these assumptions, the predictive model gives the urea concentration profile in all areas indicated in Figure 5. Into the bulk, the anolyte is assumed to be perfectly stirred, and the urea concentration is therefore considered uniform in the bulk volume, Ω_B. The macroscopic balance of urea can be written as Equation (32).

$$\underset{z\le 0}{\Omega_B} \quad \underset{\text{Accumulation flux}+\text{Diffusion flux}+(\text{Feed}+\text{Output})_{\text{flux in continuous reactor}}=0}{V^{\text{bulk}}\times\frac{\partial\left[CO(NH_2)_2\right]_{z\le 0}}{\partial t}+\left[D_{\text{urea,w}}\times S_{\text{electrode}}\times\frac{\partial\left[CO(NH_2)_2\right]}{\partial z}\right]_{z=0}+Q\times\left(\left[CO(NH_2)_2\right]_{\text{Feed}}-\left[CO(NH_2)_2\right]_{\text{Output}}\right)=0} \tag{32}$$

where Q is the volumetric flow rate ($m^3\,s^{-1}$).

In the present work, the results are obtained in a batch electrolyzer ($Q=0$). Unlike in Ω_B, the urea concentration in the diffusion film Ω_F, is subject to spatial variation caused by the urea diffusion phenomenon due to the chemical reaction in Ω_{EC}. The microscopic mass balance can be written as Equation (33).

$$\underset{0\le z\le\delta}{\Omega_F} \quad \underset{\text{Accumulation flux}+\text{Diffusion flux}=0}{(S_{\text{electrode}}\times\delta)\times\left[\frac{\partial\left[CO(NH_2)_2\right]}{\partial t}-\left[D_{\text{urea,w}}\times\frac{\partial^2\left[CO(NH_2)_2\right]}{\partial x^2}\right]\right]=0} \tag{33}$$

In the Ω_{EC} area, the coupling of the HCR to the urea diffusion into the porous solid is the main occurring phenomena. The microscopic mass balance can be written according to Equation (34).

$$\underset{\delta\le z\le\delta+\mu}{\Omega_{EC}} \quad \underset{\text{Accumulation flux}+\text{Chemical reaction flux}+\text{Diffusion effective flux}=0}{(S_{\text{electrode}}\times\mu)\times\left[\frac{\partial\left[CO(NH_2)_2\right]}{\partial t}+S_{\text{electrode}}\times r_{E_X}-D^{\text{eff}}_{\text{urea,w}}\times\frac{\partial^2\left[CO(NH_2)_2\right]}{\partial x^2}\right]=0} \tag{34}$$

Equation (34) represents a classical situation of a boundary value problem (shooting method) and its resolution is well documented in other works.[62,63] The resolution state of the model is a pseudo-steady state where the resolution is established by a succession of steady states, in the mass transport area as well as the electroactive layer, and a transient state in the bulk. The model resolution method is presented in Section S7.

4.1.3 | Boundary and initial conditions

The following initial and boundary conditions are applied:

(i) At an initial time, the urea concentration is assumed to be uniform throughout the whole system and equal to the initial concentration in the volume according to Equation (35).

$$\underset{t=0}{\forall\Omega} \quad C(z,0)=C_{\text{ini}} \tag{35}$$

(ii) It is considered that the urea does not directly react at the electrode neither with $Ni(OH)_2$ nor Ni; therefore, the mass flux arriving at the surface of the metal electrode Λ_E and at both frontiers Λ_P of the system, are assumed to zero according to Equation (36).

$$\underset{\forall t}{\forall\Lambda_E,\Lambda_P} \quad \left.\frac{\partial\left[CO(NH_2)_2\right]}{\partial z}\right|_{z=\Lambda_E,\Lambda_P}=0 \tag{36}$$

(iii) The continuity of the concentrations in each Ω domain, especially in the Ω_{EC} area, is ensured by the equality of the concentrations at each Λ boundary of the system following the Equations (37) and (38):

$$\forall t \quad C_{\Omega_B,\Lambda_{BF}}(0,t)=C_{\Omega_F,\Lambda_{BF}}(0,t) \tag{37}$$

$$C_{\Omega_F,\Lambda_{FEC}}(\delta,t)=C_{\Omega_{EC},\Lambda_{FEC}}(\delta,t) \tag{38}$$

(iv) Since the mass transport properties are significantly different in the domains Ω_F and Ω_{EC} (diffusion constant, thickness, concentration continuity), the equality of urea flux can be described as Equation (39).

$$\forall t \quad \frac{D_{\text{urea,w}}}{\delta}\times\left.\frac{\partial\left[CO(NH_2)_2\right]}{\partial z}\right|_{z=\Lambda_{FEC}}^{\Omega_F}=\frac{D^{\text{eff}}_{\text{urea,w}}}{\mu}\times\left.\frac{\partial\left[CO(NH_2)_2\right]}{\partial z}\right|_{z=\Lambda_{FEC}}^{\Omega_{EC}} \tag{39}$$

These changes can be expressed according to a Biot dimensionless number as shown in Equation (40).

$$\text{Bi}=\frac{k_{m,\Omega_F}}{k_{m,\Omega_{EC}}}=\frac{D_{\text{urea,w}}}{\delta}\times\frac{\mu}{D^{\text{eff}}_{\text{urea,w}}} \tag{40}$$

where k_m is the mass transport coefficient ($m\,s^{-1}$)

4.2 | Comparison between predictions and experimental data

4.2.1 | Thicknesses of the diffusion film and the electrocatalytic layer

Two physical dimensions of the system need to be determined prior to the application of the model: the thickness of the diffusion layer, δ, and the thickness of the electrocatalytic layer, μ.

Concerning the diffusion layer, the anodic oxidation limit current, observed on the urea diffusion plateau, is proportional to the concentration of the electroactive species. Here, nickel(III) is the electroactive specie, but its concentration will vary proportionally to that of urea according the catalytic cycle already mentioned in the previous section. Then, the following Equation (41) can be applied.

$$\delta = \frac{n \times \mathcal{F} \times D_{\text{urea,w}} \times \left[CO(NH_2)_2\right]^{\text{bulk}}}{j^{\infty}_{\text{plateau}}} \tag{41}$$

where $j^{\infty}_{\text{plateau}}$ is the limit current density current measured at the diffusion plateau in steady state (A m^{-2}) at a potential varying from 0.51 to 0.55 V (refer to Figure 3), n the number of exchanged electrons (dimensionless, 1 in case of nickel(III)/nickel(II)). Considering the values obtained in Figure 3A for the lowest urea concentration (where the concentration of urea at the electrode is close to 0, the molar flux arriving at the electrode becomes constant), a value of $\delta = (3.4 \pm 0.2) \times 10^{-5}$ m is determined.

The thickness of the electrocatalytic layer has been estimated in our previous study,[30] by determining the charge transferred during an *i*–*E* curve plotted using a massive nickel electrode in a 1 mol L^{-1} KOH solution; its value is equal to $\mu = (4.9 \pm 0.4) \times 10^{-8}$ m. This calculation leads to an estimation of 9.74×10^{20} sites m^{-2} of electrode, available at the surface.

4.2.2 | Urea electrolysis on nickel electrode: case results and comparison

In order to evaluate the veracity of the model, the experimentally measured urea concentrations in the bulk for various electrolyzes for which high conversions are achieved, will be considered and compared to the ones predicted by the model.

Figure 6 illustrates the spatio-temporal profiles of the urea concentration predicted by the model. The three spatial zones are quite distinct and well represented, allowing a good understanding of the involved processes (Ω_B, Ω_F: transport phenomena/Ω_{EC}: transport phenomena and heterogeneous reaction). A nonlinear time scale is represented for better readability of the phenomena occurring.

In the reaction area Ω_{EC}, the flux at the metal electrode (at $z = \delta + \mu$) equals zero. The concentration in this Ω_{EC} zone starts to decrease according to a nonlinear profile and tends towards a pseudo-steady state until the chemical regime competes with the diffusion flux from the diffusion film Ω_F. A linear concentration profile in the Ω_F zone is thus obtained.

In the bulk area Ω_B, the assumption of a perfectly stirred batch reactor is equivalent to an identical concentration at all points (at $z < 0$). The breaking slope observed at $z = \delta$ is representative of the urea fluxes transfer to the electrode. They indicate the discontinuities in the urea fluxes between the two media: liquid Ω_F and the catalytic Ω_{EC} layer of NiOOH/Ni(OH)$_2$. Both layers exhibit different mass transport properties (diffusion constant, thickness, concentration continuity) according to the Biot number in Equation (40). In the experimental conditions related to Figure 6, and at a KOH concentration of 5 mol L^{-1}, this ratio between the mass transfer constants in the diffusion film and in the electrocatalytic layer, respectively, is estimated to be 112, thus reflecting a diffusional limitation in the porous zone compared to the diffusion film.

The inset in Figure 6 illustrates the simulated temporal evolution of the urea concentration in the bulk (continuous line), and a good

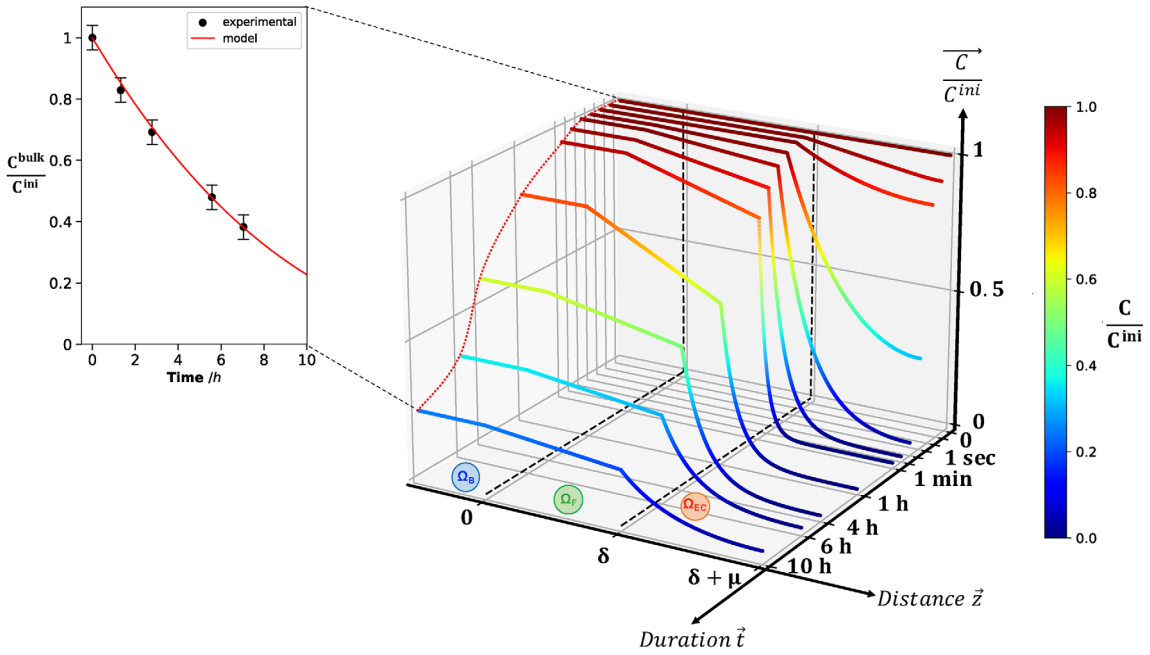

FIGURE 6 Spatio-temporal profiles of the urea concentration during a potentiostatic electrolysis at 0.55 V of a 0.33 mol L^{-1} urea solution in alkaline media (5 mol L^{-1} KOH), on nickel massive electrode. Inset: dimensionless urea concentrations in the bulk Ω_B measured experimentally (black filled circles) and predicted by the *m* odel (red line).

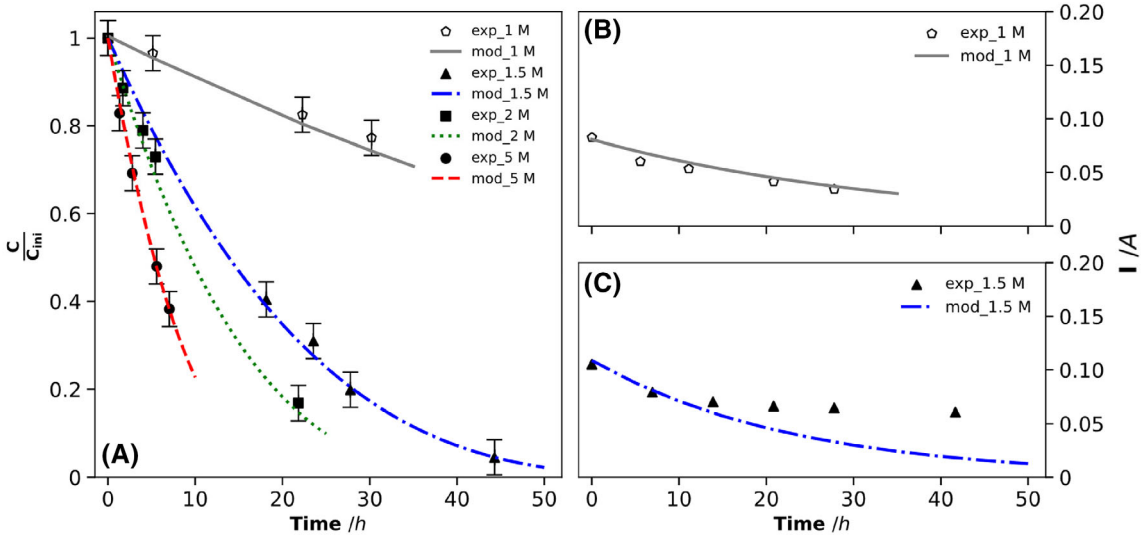

FIGURE 7 (A) Temporal variations of the normalized urea concentration in the bulk during potentiostatic electrolysis on nickel massive electrode in alkaline media. Experimental results are plotted for different KOH concentrations: 1 mol L^{-1} (⬠), 1.5 mol L^{-1} (●), 2 mol L^{-1} (■) and 5 mol L^{-1} (▲). Filled symbols are obtained with an *S*/*V* ratio of 8 m^{-1}. The unfilled symbols are obtained with an *S*/*V* ratio equal to 20 m^{-1}. The lines represent the temporal profiles of the urea concentration predicted by the model at each KOH concentration. (B) and (C) Experimental and predicted profiles of the current intensity during electrolysis with a distance between electrodes of (B) 15 cm using a H-type cell without separator and (C) 3 cm using an undivided Metrohm type-cell.

correlation is observed with the experimental points obtained in our previous work.[30]

Figure 7A compares the predicted (continuous line) and experimental (dots) normalized urea concentrations in the bulk, obtained during electrolyzes at different KOH concentrations, using two *S*/*V* ratios, where significant conversion rates of urea were reached. Data obtained for a *S*/*V* ratio of 8 are extracted from our previous work.[30] In addition to examining the validity of the model for an enhanced value of *S*/*V* ratio, an alkaline electrolysis was carried out using an anode surface of 26 cm^2 in 130 mL of electrolyte. A good correlation is observed between the experiments and the model since the maximum deviation of urea concentration is observed at 6%.

An additional validation of the model is performed by comparing the temporal variation of the current predicted by the model according to Equation (42) with the experimental one.

$$\begin{aligned}&\text{Electrogenerated } Ni^{(III)} \text{ flux} = 6 \times \text{Urea chemically reacted flux}\\ &I = n\mathcal{F}SV\nu_{Ni^{(III)}}\int_{z=\delta}^{z=\delta+\mu} r_{E\chi}(z)\times dz\\ &= \left[n\mathcal{F}V\nu_{Ni^{(III)}}k_{E\chi}\times[OH^-]^{\beta_{E\chi}}\times(S_{electrode})^{\gamma_{E\chi}+1}\right]\\ &\quad\times\int_{z=\delta}^{z=\delta+\mu}\left[CO(NH_2)_2\right]^{\alpha_{E\chi}}\times dz\end{aligned} \tag{42}$$

As shown in Figure 7B, the model predicts the current with a maximum deviation of 4%, thus implying that the main assumption considering a constant temporal superficial concentration of nickel(III) would be verified.

Results of electrolysis indicated in Figure 7C were obtained using an undivided Metrohm type cell, containing a strongly stirred (1000 rpm) solution. In these conditions, the electrogenerated hydrogen at the cathode (diameter <1 mm) is dispersed in the bulk, and consequently in the immediate environment of the anode. Strong dispersion of gaseous H_2 increases the gas/liquid interface and facilitates its dissolution (the stationary concentration of hydrogen can achieve its solubility). Under the applied anodic potential (0.55 V), the dissolved hydrogen can be oxidized, and in these conditions the observed current is composed of:

(i) the urea oxidation current (temporally decreasing);
(ii) the hydrogen oxidation current[64–66] induced by the reaction Equation (43), that first increases until the steady state is reached, that is, a constant gaseous H_2 flux arrived at the anode area.

$$H_2 + 2OH^- \rightarrow 2H_2O + 2e^- \tag{43}$$

These facts explain the observed difference of the current between the model and the experimental data, which varies from 1% to 80%. Note that, this difference will decrease as a function of time. Indeed, as the urea concentration is depleted, the corresponding fraction of anodic current is decreased, thus implying that the overall current will decrease. In these conditions the hydrogen electrogenerated flux at the cathode decreases.

As the hydrogen is not maintained in the reactor, its contribution to the anode current will also decrease until it is canceled

(simultaneously to urea). The difference in current intensity between the theoretical and experimental data corresponds to the "lost" current, due to the absence of a physical separator.

This undesirable oxidation of hydrogen, which can be considered as a loss of energy efficiency, is a key factor for controlling the thoughtful design of a UEO reactor as already discussed by Hankin et al.[67]

5 | CONCLUSIONS

This work enabled to highlighting and characterizing the kinetics of indirect urea electrooxidation on active nickel(III) sites in an alkaline medium. NiOOH particles, synthesized from commercial $Ni(OH)_2$ powder using NaOCl, were characterized by SEM, BET, XRD, and particle size analysis. They exhibited spherical shapes and their content in nickel(III) reached 80%. Compared to $Ni(OH)_2$ solids, the crystallinity of the synthesized NiOOH particles appears to be much lower than that of the starting powder, reflecting a core–shell geometry. The particles after synthesis, were composed of an amorphous NiOOH shell and a $Ni(OH)_2$ core.

Firstly, the kinetic study was performed using chemically synthesized nickel(III) particles. By using the method of initial rate of OH^- disappearance, the partial reaction order of urea was evaluated at 0.3, highlighting a limitation of the urea adsorption on the active sites of nickel. Subsequently, the partial orders of 0.6 and 1.9, respectively attributed to hydroxide ions and nickel active sites, were determined using the same type of experimental measurements. The dependence of the kinetic rate on hydroxide ions appeared to be low, whereas it was higher for nickel ($\gamma_\chi \approx 2$). Although more experiments would be required to precisely identify the reaction mechanism, an order of 2 against the nickel(III) suggests that urea would bind to two nickel sites either (i) via both amine groups or (ii) via one of the amine groups and the ketone group. Besides, this low dependence of the kinetic rate to dissolved species' concentrations would suggest possible mass transport limitations in the solid spherical particles; indeed, after the consumption of nickel(III), the transformed urea or even the by-products must desorb, and find another nickel(III) available to absorb, to pursue the oxidative process. Moreover, the performed BET analysis showed particles having a low specific surface area ($8.51\ m^2\ g^{-1}$), which would tend to incriminate limitation by the mass transport into the particles. This initial kinetic law did not consider the effect of the urea oxidized intermediates on OH^- or nickel(III) consumption, as their initial concentration was close to zero. Since the limitation of the overall process, at least initially, appears to be due to adsorption, these intermediates do not accumulate; they rapidly convert to observed products, and therefore do not affect the kinetic rate. This fact was validated by integration as a function of time, of the initial kinetic law, that is, for higher conversion rates. The obtained theoretical variation of the OH^- concentration was successfully compared with the experimental one (maximum deviation of 6%).

Second, the kinetics of indirect electrooxidation of urea was studied by polarizing a massive nickel electrode which enabled the formation of a catalytic layer $NiOOH/Ni(OH)_2$, and thus ensured the urea oxidation thanks to the electrochemical continuous regeneration of the nickel(III) actives sites. Under these assumptions, the kinetic rate law showed a partial order of urea close to the previous value (i.e., 0.3). However, the order of the nickel surface was found to be high ($\gamma_{E\chi} \approx 5$), signifying that the adsorption of urea onto nickel(III) sites was followed by complete oxidation of this urea by five electrochemically generated nickel(III) sites, almost instantaneously due to potentiostatic polarization of the anode at the required potential.

Coupled with the previously performed mass balances, carried out during preparative electrolyzes (which demonstrated the presence of various by-products in the liquid phase), the present kinetic study made it possible to create a relatively complete multipathway mechanism (22 sequential steps, 4 different ways and 5 urea oxidation products), able to describe the process of indirect electrooxidation of urea.

Finally, this kinetic study was inserted into a more general predictive model combining (i) mass transport phenomena, in a liquid film and in a solid porous catalytic layer with (ii) indirect electrocatalytic chemical reaction occurring in the previous layer, and finally (iii) assisted by the quasi-instantaneous regeneration of the reaction driving factor, that is, the nickel(III) catalytic sites. The resolution of the established model on the basis of the shooting method enabled the prediction of spatio-temporal urea concentration profiles for various operating conditions. These predicted results were compared to the experimental ones for different hydroxide concentrations and *S*/*V* ratio. A satisfactory correlation was observed with low (<5%) deviations, thus opening interesting perspectives for further larger-scale operations for urea mineralization.

NOTATION

Letters

CE	counter electrode
E	applied potential (mV vs. Hg/HgO)
ER	electrogenerated reaction
$\mathcal{F}$	Faraday's constant (96,500 C mol^{-1})
I	current (A)
j	current density (A m^{-2})
HCR	heterocatalytic chemical reaction
n	number of exchanged electron (dimensionless)
Q	flowrate ($m^3\ s^{-1}$)
t	time (s)
T	temperature (K)
UEO	urea electrooxidation
V, V_B	suspension volume/electrolyte volume (m^3)
WE	working electrode
x	length of the electrode (m)
X	conversion rate (dimensionless)
z	distance to the electrode (m)
δ	diffusion layer thickness (m)
ε	nickel accessibility factor (dimensionless)
μ	mixed oxides layer length (m)
τ	tortuosity of the electrocatalytic layer (dimensionless)

ω	porosity of electrocatalytic layer (dimensionless)
θ	scattering angle (°)
ξ	extent of reaction (mol)

Subscripts

d_{10}, d_{50}, d_{90}	percentile value diameters (µm)
d_{32}, d_{43}	Sauter Mean diameter and De Brouckere Mean diameter (µm)
$D_{i,w}$	diffusion binary coefficient of the specie i in the water ($m^2\ s^{-1}$)
$D_{i,w}^{eff}$	effective diffusion binary coefficient of the specie i in the water in porous media ($m^2\ s^{-1}$)
$I_{plateau}$	limiting current, observed at the plateau signal (A)
$I_{plateau}^{\infty}$	limiting current, observed at the plateau signal in steady state (A)
$j_{plateau}^{\infty}$	limiting density current, observed at the plateau signal in steady state ($A\ m^{-2}$)
$k_{app}, k'_{app}, k''_{app}$	apparent constants of $r_\chi(t)$ (variable unit)
k_m	mass transport coefficient ($m\ s^{-1}$)
k_χ	reaction rate constant of r_χ ($mol^{1-\alpha_\chi-\beta_\chi-\gamma_\chi}\ m^{3(\alpha_\chi+\beta_\chi)-3}.(g_{cat}\ s)^{-1}$)
$k_{E\chi}$	reaction rate constant of $r_{E\chi}$ ($mol^{1-\alpha_{E\chi}-\beta_{E\chi}-\gamma_{E\chi}}.m^{3(\alpha_{E\chi}+\beta_{E\chi})-2}.s^{-1}$)
m_{cat}	mass of powder (g)
$M_{Ni^{III}}$	NiOOH molar mass ($g\ mol^{-1}$)
n_i	amount of substance i (mol)
r_χ	instantaneous reaction rate for powder nickel(III) study ($mol\ m^3\ (g_{cat}\ s)^{-1}$)
r_χ^0	initial rate of r_χ ($mol\ m^3\ (g_{cat}\ s)^{-1}$)
$r_{E\chi}$	kinetic law obtained on electrogenerated nickel(III) sites ($mol\ m^2_{electrode}\ s^{-1}$)
$S_{electrode}$	electrode surface (m^2)
$\alpha_\chi, \beta_\chi, \gamma_\chi$	partial orders of urea, hydroxide, and nickel respectively (dimensionless) determined with nickel-oxides synthesized powders
$\alpha_{E\chi}, \beta_{E\chi}, \gamma_{E\chi}$	partial orders of urea, hydroxide, and nickel respectively (dimensionless) determined with nickel-oxides electrodes
Γ_i	superficial concentration of the nickel at the oxidation state *i* ($mol\ m^{-2}$)
Λ_i	model border *i*
ρ_{cat}	mass concentration of nickel(III) per unit of volume ($g_{cat}\ m^{-3}$)
$\Omega_B, \Omega_F, \Omega_{EC}$	model domains respectively, bulk, diffusion film and electrocatalytic layer
ν_i	stochiometric number of the reactant i (dimensionless)
ν_{scan}	potential scan rate ($V\ s^{-1}$)

Superscripts

C^{bulk}	bulk urea concentration ($mol\ m^{-3}$)
$C^{electrode}$	electrode urea concentration ($mol\ m^{-3}$)
C^F	urea concentration at the interface between diffusion film and electrocatalytic layer ($mol\ m^{-3}$)

AUTHOR CONTRIBUTIONS

Guillaume Hopsort: Conceptualization (lead); data curation (lead); formal analysis (lead); investigation (lead); methodology (lead); validation (lead); visualization (lead); writing – original draft (lead). **Laure Latapie:** Conceptualization (supporting); formal analysis (supporting); investigation (supporting); methodology (supporting); resources (supporting). **Karine Groenen-Serrano:** Conceptualization (equal); formal analysis (equal); investigation (equal); supervision (equal); validation (equal); writing – review and editing (equal). **Karine Loubiere:** Conceptualization (equal); formal analysis (equal); investigation (equal); supervision (equal); validation (equal); writing – review and editing (equal). **Theodore Tzedakis:** Conceptualization (lead); formal analysis (lead); funding acquisition (lead); investigation (lead); methodology (lead); project administration (lead); supervision (lead); validation (lead); writing – review and editing (lead).

ACKNOWLEDGMENTS

This work was supported by the French National Research Agency (proposal HYUREA ANR-19-CE04-0009). The authors would like to thank S. Mallet-Ladeira (CNRS, LCC, Toulouse) for the DRX analysis and useful explanations about this method, D. Pereira Do Carmo, master trainee (LGC, Toulouse) for her help concerning some experiments, Pr. P. Bacchin and Dr. F. Chauvet for their useful discussions concerning the numerical methods (LGC, Toulouse).

DATA AVAILABILITY STATEMENT

All data required to evaluate the conclusions in this paper are present in the paper itself and/or the Supplementary Materials. Additional data that support the findings of this study are available from the corresponding author, upon request. Error bars (where shown) in Figures 1 and 7 show the spread of data observed in duplicate measurements, where independent samples were tested for each measurement. Experimental data shown without error bars are from mean of individual experimental measurements.

ORCID

Guillaume Hopsort https://orcid.org/0000-0002-5619-9667
Karine Groenen Serrano https://orcid.org/0000-0002-1423-6159
Karine Loubière https://orcid.org/0000-0001-6245-2844
Theodore Tzedakis https://orcid.org/0000-0002-9222-4487

REFERENCES

1. Qadir M, Drechsel P, Jiménez Cisneros B, et al. Global and regional potential of wastewater as a water, nutrient and energy source. *Nat Res Forum*. 2020;44:40-51. doi:10.1111/1477-8947.12187
2. Bouatra S, Aziat F, Mandal R, et al. The human urine metabolome. Dzeja P (Ed.). *PLoS One*. 2013;8:e73076. doi:10.1371/journal.pone.0073076
3. Larsen TA, Gujer W. Separate management of anthropogenic nutrient solutions (human urine). *Water Sci Technol*. 1996;34:87-94. doi:10.2166/wst.1996.0420
4. Boggs BK, King RL, Botte GG. Urea electrolysis: direct hydrogen production from urine. *Chem Commun*. 2009;32:4859-4861. doi:10.1039/b905974a

5. Kim J, Choi WJK, Choi J, Hoffmann MR, Park H. Electrolysis of urea and urine for solar hydrogen. *Catal Today*. 2013;199:2-7. doi:10.1016/j.cattod.2012.02.009
6. King RL, Botte GG. Investigation of multi-metal catalysts for stable hydrogen production via urea electrolysis. *J Power Sources*. 2011;196:9579-9584. doi:10.1016/j.jpowsour.2011.06.079
7. Amstutz V, Katsaounis A, Kapalka A, Comninellis C, Udert KM. Effects of carbonate on the electrolytic removal of ammonia and urea from urine with thermally prepared IrO_2 electrodes. *J Appl Electrochem*. 2012;42(9):787-795. doi:10.1007/s10800-012-0444-y
8. Santoro C, Garcia MJS, Walter XA, et al. Urine in bioelectrochemical systems: an overall review. *ChemElectroChem*. 2020;7:1312-1331. doi:10.1002/celc.201901995
9. Kim OH, Choi HJ, Kang SY, et al. Towards outstanding performance of direct urea fuel cells through optimization of anode catalyst layer and operating conditions. *J Electroanal Chem*. 2022;921:116661. doi:10.1016/j.jelechem.2022.116661
10. Basumatary P, Konwar D, Yoon YS. A novel Ni Cu/ZnO@MWCNT anode employed in urea fuel cell to attain superior performances. *Electrochim Acta*. 2018;261:78-85. doi:10.1016/j.electacta.2017.12.123
11. Ye K, Wang G, Cao D, Wang G. Recent advances in the electro-oxidation of urea for direct urea fuel cell and urea electrolysis. *Top Curr Chem*. 2018;376:42. doi:10.1007/s41061-018-0219-y
12. Lan R, Tao S, Irvine JTS. A direct urea fuel cell – power from fertiliser and waste. *Energ Environ Sci*. 2010;3:438. doi:10.1039/b924786f
13. Sayed ET, Eisa T, Mohamed HO, et al. Direct urea fuel cells: challenges and opportunities. *J Power Sources*. 2019;417:159-175. doi:10.1016/j.jpowsour.2018.12.024
14. Zhu B, Liang Z, Zou R. Designing advanced catalysts for energy conversion based on urea oxidation reaction. *Small*. 2020;16:e1906133. doi:10.1002/smll.201906133
15. Sun X, Ding R. Recent progress with electrocatalysts for urea electrolysis in alkaline media for energy-saving hydrogen production. *Cat Sci Technol*. 2020;10:1567-1581. doi:10.1039/C9CY02618E
16. Ye K, Zhang D, Guo F, Cheng K, Wang G, Cao D. Highly porous nickel@carbon sponge as a novel type of three-dimensional anode with low cost for high catalytic performance of urea electro-oxidation in alkaline medium. *J Power Sources*. 2015;283:408-415. doi:10.1016/j.jpowsour.2015.02.149
17. Ding R, Qi L, Jia M, Wang H. Facile synthesis of mesoporous spinel $NiCo_2O_4$ efficient electrocatalysts for urea electro-oxidation. *Nanoscale*. 2014;6:1369-1376. doi:10.1039/C3NR05359H
18. Li J, Wang S, Chang J, Feng L. A review of Ni based powder catalyst for urea oxidation in assisting water splitting reaction. *Adv Powder Mater*. 2022;1:100030. doi:10.1016/j.apmate.2022.01.003
19. Yan W, Wang D, Botte GG. Nickel and cobalt bimetallic hydroxide catalysts for urea electro-oxidation. *Electrochim Acta*. 2012;61:25-30. doi:10.1016/j.electacta.2011.11.044
20. Vedharathinam V, Botte GG. Direct evidence of the mechanism for the electro-oxidation of urea on $Ni(OH)_2$ catalyst in alkaline medium. *Electrochim Acta*. 2013;108:660-665. doi:10.1016/j.electacta.2013.06.137
21. Daramola DA, Singh D, Botte GG. Dissociation rates of urea in the presence of NiOOH catalyst: a DFT analysis. *J Phys Chem*. 2010;114:11513-11521. doi:10.1021/jp105159t
22. Chakrabarty S, Offen-Polak I, Burshtein TY, Farber EM, Kornblum L, Eisenberg D. Urea oxidation electrocatalysis on nickel hydroxide: the role of disorder. *J Solid State Electrochem*. 2020;25:159-171. doi:10.1007/s10008-020-04744-6
23. Li J, Zhang J, Yang JH. Research progress and applications of nickel-based catalysts for electrooxidation of urea. *Int J Hydrogen Energy*. 2022;47:7693-7712. doi:10.1016/j.ijhydene.2021.12.099
24. Li J, Li J, Liu T, et al. Deciphering and suppressing over-oxidized nitrogen in nickel-catalyzed urea electrolysis. *Angew Chem Int Ed*. 2021;60:26656-26662. doi:10.1002/anie.202107886
25. Tatarchuk SW, Medvedev JJ, Li F, Tobolovskaya Y, Klinkova A. Angew. Chem. Int. Ed. 2022, 61, e202209839. *Angew Chem*. 2022;134:e202209839. doi:10.1002/ange.202209839
26. Zaher A, Shehata N. Recent advances and challenges in management of urea wastewater: a mini review. *IOP Conf Ser Mater Sci Eng*. 2021;1046:012021. doi:10.1088/1757-899X/1046/1/012021
27. Ma Y, Ma C, Wang Y, Wang K. Advanced nickel-based catalysts for urea oxidation reaction: challenges and developments. *Catalysts*. 2022;12:337. doi:10.3390/catal12030337
28. Vedharathinam V, Botte GG. Understanding the electro-catalytic oxidation mechanism of urea on nickel electrodes in alkaline medium. *Electrochim Acta*. 2012;81:292-300. doi:10.1016/j.electacta.2012.07.007
29. Singh RK, Schechter A. Electrochemical investigation of urea oxidation reaction on β-$Ni(OH)_2$ and $Ni/Ni(OH)_2$. *Electrochim Acta*. 2018;278:405-411. doi:10.1016/j.electacta.2018.05.049
30. Hopsort G, Carmo DPD, Latapie L, Loubière K, Serrano KG, Tzedakis T. Progress toward a better understanding of the urea oxidation by electromediation of Ni(III)/Ni(II) system in alkaline media. *Electrochim Acta*. 2023;442:141898. doi:10.1016/j.electacta.2023.141898
31. Wang X, Li J, Duan Y, et al. Electrochemical urea oxidation in different environment: from mechanism to devices. *ChemCatChem*. 2022;14:e202101906. doi:10.1002/cctc.202101906
32. Sun W, Zhang M, Li J, Peng C. Solar-driven catalytic urea oxidation for environmental remediation and energy recovery. *ChemSusChem*. 2022;8:e202201263. doi:10.1002/cssc.202201263
33. Pan J, Sun Y, Wan P, Wang Z, Liu X. Synthesis, characterization and electrochemical performance of battery grade NiOOH. *Electrochem Commun*. 2005;7:857-862. doi:10.1016/j.elecom.2005.05.004
34. Thimmasandra NR. Effect of crystallinity of β- and βbc-nickel hydroxide samples on chemical cycling. Kalyanaraman R (Ed.). *Indian J Mater Sci*. 2015;2015:1-7. doi:10.1155/2015/820193
35. Shangguan E, Chang Z, Tang H, Yuan X, Wang H. Preparation of nickel oxyhydroxide by a new electrolysis method using spherical β-$Ni(OH)_2$. *Int J Hydrogen Energy*. 2010;35:3214-3220. doi:10.1016/j.ijhydene.2010.01.098
36. Kashani Motlagh MM, Youzbashi AA, Hashemzadeh F, Sabaghzadeh L. Structural properties of nickel hydroxide/oxyhydroxide and oxide nanoparticles obtained by microwave-assisted oxidation technique. *Powder Technol*. 2013;237:562-568. doi:10.1016/j.powtec.2012.12.047
37. Bantignies JL, Deabate S, Righi A, et al. New insight into the vibrational behavior of nickel hydroxide and Oxyhydroxide using inelastic neutron scattering, far/mid-infrared and Raman spectroscopies. *J Phys Chem C*. 2008;112:2193-2201. doi:10.1021/jp075819e
38. Hall DS, Lockwood DJ, Bock C, MacDougall BR. Nickel hydroxides and related materials: a review of their structures, synthesis and properties. *Proc R Soc A: Math Phys Eng Sci*. 2015;471:20140792. doi:10.1098/rspa.2014.0792
39. Fu XZ, Zhu YJ, Xu QC, et al. Nickel oxyhydroxides with various oxidation states prepared by chemical oxidation of spherical β-$Ni(OH)_2$. *Solid State Ion*. 2007;178:987-993. doi:10.1016/j.ssi.2007.04.011
40. Garcia-Segura S, Nienhauser AB, Fajardo AS, et al. Disparities between experimental and environmental conditions: research steps toward making electrochemical water treatment a reality. *Curr Opin Electrochem*. 2020;22:9-16. doi:10.1016/j.coelec.2020.03.001
41. Pardue HL. Kinetic aspects of analytical chemistry. *Anal Chim Acta*. 1989;216:216-107. doi:10.1016/S0003-2670(00)82005-X
42. Casado J, Lopez-Quintela MA, Lorenzo-Barral FM. The initial rate method in chemical kinetics: evaluation and experimental illustration. *J Chem Educ*. 1986;63:450. doi:10.1021/ed063p450
43. Alex C, Shukla G, John NS. Introduction of surface defects in NiO with effective removal of adsorbed catalyst poisons for improved electrochemical urea oxidation. *Electrochim Acta*. 2021;385:138425. doi:10.1016/j.electacta.2021.138425

44. Zhao Z, Wang H, Tan H, et al. Deciphering the active origin for urea oxidation reaction over nitrogen penetrated nickel nanoparticles embedded in carbon nanotubes. *J Colloid Interface Sci*. 2022;626:740-751. doi:10.1016/j.jcis.2022.06.131
45. Anuratha KS, Rinawati M, Wu TH, Yeh MH, Lin JY. Recent development of nickel-based Electrocatalysts for urea electrolysis in alkaline solution. *Nanomaterials*. 2022;12:2970. doi:10.3390/nano12172970
46. Tong Y, Jin K, Bei H, et al. Local lattice distortion in NiCoCr, FeCoNiCr and FeCoNiCrMn concentrated alloys investigated by synchrotron X-ray diffraction. *Mater Des*. 2018;155:1-7. doi:10.1016/j.matdes.2018.05.056
47. Hameed B, Din A, Ahmad A. Adsorption of methylene blue onto bamboo-based activated carbon: kinetics and equilibrium studies. *J Hazard Mater*. 2007;141:819-825. doi:10.1016/j.jhazmat.2006.07.049
48. Bielinski C, Le N, Kaoui B. Unsteady mass transfer from a core–shell cylinder in crossflow. *Phys Rev Fluids*. 2021;6:023501. doi:10.1103/PhysRevFluids.6.023501
49. Thomas LC, Dorizas A, Mech E. Comparison of integration vs. fixed-time methods for kinetic analyses. *Anal Lett*. 1989;22:989-997. doi:10.1080/00032718908051382
50. Chen W, Xie C, Wang Y, et al. Activity origins and design principles of nickel-based catalysts for nucleophile electrooxidation. *Chemistry*. 2020;6:2974-2993. doi:10.1016/j.chempr.2020.07.022
51. Chen W, Wang Y, Wu B, et al. Activated Ni-OH bond in catalyst facilitates nucleophile oxidation reaction. *Adv Mater*. 2022;34:e2105320. doi:10.1002/adma.202105320
52. Qi Y, Zhang Y, Yang L, et al. Insights into the activity of nickel boride/nickel heterostructures for efficient methanol electrooxidation. *Nat Commun*. 2022;13:4602. doi:10.1038/s41467-022-32443-5
53. Ge J, Liu Z, Guan M, et al. Investigation of the electrocatalytic mechanisms of urea oxidation reaction on the surface of transition metal oxides. *J Colloid Interface Sci*. 2022;620:442-453. doi:10.1016/j.jcis.2022.03.152
54. Mazzei L, Musiani F, Ciurli S. The structure-based reaction mechanism of urease, a nickel dependent enzyme: tale of a long debate. *JBIC J Biol Inorg Chem*. 2020;25:829-845. doi:10.1007/s00775-020-01808-w
55. Mazzei L, Cianci M, Benini S, Ciurli S. The structure of the elusive urease–urea complex unveils the mechanism of a paradigmatic nickel-dependent enzyme. *Angew Chem Int Ed*. 2019;58:7415-7419. doi:10.1002/anie.201903565
56. Choueiri RM, Tatarchuk SW, Klinkova A, Chen LD. Mechanism of ammonia oxidation to dinitrogen, nitrite, and nitrate on β-$Ni(OH)_2$ from first-principles simulations. *Electrochem Sci Adv*. 2022;2:e2100142. doi:10.1002/elsa.202100142
57. Shih YJ, Huang YH, Huang CP. Electrocatalytic ammonia oxidation over a nickel foam electrode: role of $Ni(OH)_{2(s)}$—$NiOOH_{(s)}$ nanocatalysts. *Electrochim Acta*. 2018;263:261-271. doi:10.1016/j.electacta.2018.01.045
58. Medvedev JJ, Tobolovskaya Y, Medvedeva XV, Tatarchuk SW, Li F, Klinkova A. Pathways of ammonia electrooxidation on nickel hydroxide anodes and an alternative route towards recycled fertilizers. *Green Chem*. 2022;24:1578-1589. doi:10.1039/D1GC04140A
59. Zhu D, Zhang H, Miao J, et al. Strategies for designing more efficient electrocatalysts towards the urea oxidation reaction. *J Mater Chem A*. 2022;10:3296-3313. doi:10.1039/D1TA09989B
60. Xiong X, Ding D, Chen D, et al. Three-dimensional ultrathin $Ni(OH)_2$ nanosheets grown on nickel foam for high-performance supercapacitors. *Nano Energy*. 2015;11:154-161. doi:10.1016/j.nanoen.2014.10.029
61. Li L, Xu J, Lei J, et al. A one-step, cost-effective green method to in situ fabricate $Ni(OH)_2$ hexagonal platelets on Ni foam as binder-free supercapacitor electrode materials. *J Mater Chem A*. 2015;3:1953-1960. doi:10.1039/C4TA05156D
62. Lee J, Kim DH. An improved shooting method for computation of effectiveness factors in porous catalysts. *Chem Eng Sci*. 2005;60:5569-5573. doi:10.1016/j.ces.2005.05.027
63. Natesan S, Ramanujam N. 'Shooting method' for singularly perturbed one-dimensional reaction–diffusion neumann problems. *Int J Comput Math*. 1999;72:383-393. doi:10.1080/00207169908804861
64. Davydova ES, Speck FD, Paul MTY, Dekel DR, Cherevko S. Stability limits of Ni-based hydrogen oxidation electrocatalysts for anion exchange membrane fuel cells. *ACS Catal*. 2019;9:6837-6845. doi:10.1021/acscatal.9b01582
65. Zhou Z, Liu Y, Zhang J, Pang H, Zhu G. Non-precious nickel-based catalysts for hydrogen oxidation reaction in alkaline electrolyte. *Electrochem Commun*. 2020;121:106871. doi:10.1016/j.elecom.2020.106871
66. Trinke P, Haug P, Brauns J, Bensmann B, Hanke-Rauschenbach R, Turek T. Hydrogen crossover in PEM and alkaline water electrolysis: mechanisms, direct comparison and mitigation strategies. *J Electrochem Soc*. 2018;165:F502-F513. doi:10.1149/2.0541807jes
67. Hankin A, Bedoya-Lora FE, Ong CK, Alexander JC, Petter F, Kelsall GH. From millimetres to metres: the critical role of current density distributions in photo-electrochemical reactor design. *Energ Environ Sci*. 2017;10:346-360. doi:10.1039/C6EE03036J
68. Picioreanu C, Head IM, Katuri KP, van Loosdrecht MCM, Scott K. A computational model for biofilm-based microbial fuel cells. *Water Res*. 2007;41:2921-2940. doi:10.1016/j.watres.2007.04.009

SUPPORTING INFORMATION

Additional supporting information can be found online in the Supporting Information section at the end of this article.

How to cite this article: Hopsort G, Latapie L, Groenen Serrano K, Loubière K, Tzedakis T. Indirect urea electrooxidation by nickel(III) in alkaline medium: From kinetic and mechanism to reactor modeling. *AIChE J*. 2023;69(9):e18113. doi:10.1002/aic.18113